Regulation of mitochondrial morphology and function

by Stearoylation of TfR1

Senyilmaz et al.

Supplemental Information

Contents:

1. Supplementary Discussion ..... p. 1

2. Methods ..... p. 7

3. References ..... p. 44

4. Complete, uncropped western blots ..... p. 56

1. Supplementary Discussion

In animals, fatty acids are first generated as C16:0 (palmitic acid) by recursive addition of two-carbon units by fatty acid synthase [1,2]. After that, the key enzyme required for generation of very long chain fatty acids is Elovl6, which synthesizes C18 fatty acids from C16 fatty acids [1-5]. Here we show that C18:0 plays an important role in regulating mitochondrial function, in agreement with findings by many others that not only the quantity, but also the quality of fatty acids is important for determining the impact of fatty acids on organismal health (some

examples [6-9]). Indeed, *ELOVL6* knockout mice accumulate significant amounts of lipids in their livers [6,10-13], and some reports indicate they are nonetheless protected from insulin resistance [6,12-14], in agreement with the idea that not all fatty acids are functionally equivalent. Other reports did not see protection from insulin resistance [10], so additional work might shed light on the genetic or environmental conditions accounting for this discrepancy. A number of studies have linked Elovl6 to diabetes [15-17]. Since mitochondrial function and in particular mitochondrial dynamics plays a role in development of diabetes [18], it might be interesting to study whether one possible link between Elovl6 and diabetes might be via mitochondrial dynamics.

One point worth mentioning is that the effects observed here are very specific for C18:0. C12:0, C14:0, C16:0, C18:1 and C20:0 all do not promote mitochondrial fusion as C18:0 does (ED Fig. 2e-e'). Likewise, of all the alkyne and azide derivatives of C18:0 that we tested, only C17:0-azide was functionally equivalent to C18:0 in terms of mitochondrial fusion (ED Fig. 7a). In particular, C16:0-alkyne was not functionally equivalent to C18:0 despite very similar structures of these two molecules. This suggests that the acyl transferase that transfers C18:0 onto proteins is highly selective for C18:0.

Unlike *Elovl6* knockout mice which display partial embryonic lethality[10,11], *Elovl6* knockout flies are fully lethal. The lethality of *Elovl6* knockout flies can be rescued by expression of human *Elovl6*, indicating their lethality is truly due to

loss of Elovl6 activity, and not an additional phenotype. One likely reason accounting for this difference is that flies have very little C18:0 in their diet, since they eat a diet rich in carbohydrates and protein. Hence, the low levels of dietary C18:0 do not rescue the lack of endogenous C18:0 production. In fact, it is likely for this very reason that we were able to observe the phenotypes reported here. In agreement with this hypothesis, the larval lethality of *Elovl6* mutant flies is indeed rescued as soon as C18:0 is provided exogenously as a dietary supplement. In comparison, it is likely that mice obtain significantly higher levels of exogenous C18:0 in utero from their mothers, in mouse milk, and later on in regular chow. Another difference between the fly and the mammalian system is that fly Elovl6 is mitochondrially localized (Fig. 1g) whereas mammalian Elovl6 localizes to the ER [5,19]. That said, ER and mitochondria share many contact sites [20,21] where presumably lipids exchange between membranes, so that this difference might not have significant functional consequences.

One result that is counter-intuitive is that dietary C18:0 supplementation rescues phenotypes of pink and parkin mutant flies. This is counterintuitive because several reports have shown that pink and parkin mutant flies have hyper-fused mitochondria, and that the phenotypes of these flies can be ameliorated by genetic manipulations that increase fragmentation, and aggravated by manipulations that increase fusion [22-25]. This makes sense given that pink and parkin have been shown to promote mitofusin ubiquitination [26,27]. Hence C18:0 supplementation, which increases mitochondrial fusion, would not be expected to

rescue pink or parkin mutant phenotypes. Thus, although C18:0 feeding does affect mitochondrial fusion (Figures 3 and 4a), it likely also has additional effects on mitochondrial and neuronal health. Since C18:0 is acting via a signaling path that starts with TfR1 and acts via JNK and HUWE1, there are several signaling nodes downstream of C18:0 that could be affecting mitochondrial and neuronal health independently of mitochondrial morphology. For instance, C18:0 reduces JNK activation (ED Fig. 9c-d'). *Parkin* mutant flies have a strong activation of JNK in their dopaminergic neurons, and expression of dominant negative JNK restores the morphology and TH levels of these neurons [28]. Hence C18:0 feeding and parkin mutation could be interacting at the level of JNK. Furthermore, HUWE1 regulates neuronal function by additional mitofusin-independent mechanisms, for instance by ubiquitinylating the antiapoptotic factor Mcl-1 [29] or by regulating Wnt signaling [30]. Thus C18:0 can also impact neuronal health via these mitofusin-independent mechanisms.

Another result that appears counter-intuitive is an apparent increase in Mfn levels upon C18:0 removal, since increased Mfn ubiquitination should promote its turnover (ED Figs. 4a-b). For mammalian Mfn (ED Fig. 4b), it is worth noting that the Mfn immunoprecipitation (IP) seems to pull-down a particular subset of the total cellular Mfn, because the IP looks different than the "input", which is total cell lysate (ED Figure 4b). It is possible that the IP preferentially pulls-down Mfn that is not on a membrane and on its way towards degradation. If one looks at total cell lysate (the bottom panel in ED Fig. 4b), Mfn2 levels do indeed drop in

response to C18:0 removal, as would be expected. Indeed, a cyclohexamide chase experiment to look at Mfn2 half-life in cells with or without C18:0 shows that upon removal of C18:0 Mfn2 becomes less stable (ED Fig. 4d-d'). For the Drosophila protein (ED Fig. 4a) the figure is showing total animal lysates, so in this case steady-state levels of dMfn increase in the *Elovl6* mutant larvae. In an animal context, secondary consequences and homeostatic mechanisms can kick-in. For instance, we see increased expression of dMfn2 in the *dElovl6*-animals at the mRNA level (ED Fig. 4e), which could account for part of this increase. In any case, the simple take-away from ED Figures 4a-b is that upon removal of C18:0 there are differences in the post-translational modification of Mfn.

Another point worth mentioning is that the manipulations we performed rescued survival of *Elovl6* mutants through larval development to pupation. This is very significant, since the larval phases encompass the entire growth phase of the animal. That said, none of the manipulations we performed, except the genetic rescue re-expressing *Elovl6*, was able to rescue survival of *Elovl6* mutants past pupation. In particular, even dietary C18:0 supplementation did not rescue viability of *Elovl6* mutants past pupation. This suggests dElovl6 might have an additional function at the end of pupation that is independent of C18:0, perhaps relating to C18:1, since Elovl6 also elongates C16:1 to 18:1. We did not analyze this aspect of Elovl6 function in this story, since we focused on C18:0.

To our knowledge, our study is the first example whereby stearoylation of a human protein regulates its function. Previous studies have identified three plant or viral proteins that can be stearoylated[31-33] and three human proteins that are stearoylation[34-36]. Our data indicate that stearoylation of TfR1 inhibits activation of JNK, thereby preventing mitochondrial fragmentation. Interestingly, this happens also in the absence of the non-canonical TfR1 ligand gambogic acid[37-41], suggesting that either TfR1 has some basal activation also in the absence of ligand, or that other TfR1 ligands can activate it. The finding that TfR1 regulates mitochondrial morphology was completely unexpected to us, since TfR1 is a well characterized membrane receptor involved in iron uptake into cells [42-51]. To our knowledge, until now there was no obvious connection between TfR1 and regulation of mitochondrial morphology. However, in retrospect, it is reasonable that the receptor that uptakes iron into the cell is coupled to the organelle where the iron is used – mitochondria – in agreement with the burgeoning concept that there is extensive cross-talk between cells and their mitochondria [52]. Also unexpected is that C18:0 levels should be coupled to mitochondrial morphology and function. One possible explanation is that C18:0 simply serves as a proxy to the animal for availability of long chain fatty acids in general. If long chain fatty acids are not abundant, mitochondria should not beta-oxidize them. Indeed, Elovl6 knockout mice have been reported to have reduced levels of fatty acid beta-oxidation [6].

In sum, this work identifies a novel signaling route starting with regulation of the transmembrane receptor TfR1 by C18:0 and ending with altered mitochondrial fusion and function.

2. Methods

Methods related to figure panels

For Fig. 1a,synchronized 1st instar larvae were put at a defined concentration (60/vial) into vials containing either standard food or food lacking antifungal reagents (nipagin, propionic acid and phosphoric acid). Survival to pupation was quantified. Values represent averages of 4 biological replicates.

For Fig. 1b, synchronized 1st instar animals (30 per vial) were grown on food lacking antifungal agents, either in the absence or presence of rotenone (100μM), and the percentage of animals reaching pupation was quantified. Values represent the average of 3 biological replicates. Please note that survival of dElovl6 mutants is modulated by rearing density, with mildly increased survival when animals are grown at low density (30 per vial) compared to 60 per vial, likely due to competition for low levels of C18:0 present in the fly food – see Extended Data Figure 1k.

For Fig. 1c and c',,oxygen consumption was measured in inverted and permeabilized whole female larval tissues from animals grown on antifungal free food (6 larvae per sample) using Clark electrodes (Oroboros O2k High Resolution Respirometer) in respiratory buffer that is hyperoxygenated (500μM O_2) to assure oxygen supply to the tissues is not limiting. Complex I → III dependent respiration was measured by supplying Complex I substrates: 10mM proline, 10mM pyruvate, 5mM malate, 5mM glutamate and 2mM ADP. Complex (I + II) → III dependent respiration was measured by supplying Complex II substrates 10mM succinate and 15mM glycerol-3-phosphate in addition to the Complex I substrates. Values are normalized to tissue wet weight and corrected for non-mitochondrial oxygen consumption (basal respiration in the presence of the Complex III inhibitor Antimycin A). Values represent the average of 4 independent experiments.

For Fig. 1d, Ciona intestinalis alternative oxidase (AOX), which allows electrons to bypass Complexes III+IV was expressed with actin-GAL4 driver and. respiration was measured as in (c-c'). Values represent the average of 4 independent experiments.

For Fig 1e, Survival to pupation of Elovl6 mutants is fully rescued by ubiquitous expression (actin-GAL4) of PGC1α (called Spargel in Drosophila), a master regulator of mitochondrial biogenesis. Elovl6 mutants expressing PGC1α survive

to pupation at expected mendelian frequencies (Chi square test $1.97<3.841=\chi^2$ where p=0.05, n=195). Flies were grown on antifungal free food at high density.

For Fig. 1f, to show that Elovl6 mutants are fully rescued at expected mendelian frequencies by ubiquitous expression (actin-GAL4) of Ciona intestinalis alternative oxidase (AOX) which allows electrons to bypass Complexes III & IV, Chi square test was applied ($0.022<3.841=\chi^2$ where p=0.05, n=81). Flies were grown on antifungal free food at high density.

In Fig. 1g, N or C terminus tagged versions of dElovl6 (red, HA staining) was shown to colocalize with mitochondria (green, mitoGFP) by confocal microscopy.and colocalization coefficient (R=0.938) was computed by using the Image J plugin JaCoP. Scale bar 10μm. Images are representative of 4.

In Fig. 2a and a', mitochondrial morphology of female control or Elovl6 mutant larvae, fed control or C18:0 (10%) supplemented antifungal free food, was visualized with mito-GFP. Mitochondrial fragmentation was quantified by normalizing the number of mitochondrial particles to total mitochondrial area (a'). 8 optical areas from 4 animals of each genotype and food condition were quantified in a double blind fashion.

For Fig. 2b and b', *Drosophila* S2 cells grown in Serum Free Medium (SFM) Cells were treated with either control dsRNA or dsRNA targeting dElovl6, and

ranked with respect to their mitochondrial fragmentation status in a double blind fashion as indicated. Approximately 50 cells were quantified for each condition. For statisctics, Mann-Whitney test was applied.

In Fig 2c and c', human (HeLa) cells were treated for 24 hours with medium containing serum that had been delipidated by organic phase extraction. C18:0 resupplementation (100μM, conjugated to BSA) was performed during the last 2 hrs. Cells were stained with mitotracker red 45 mins before fixing and stained with DAPI after fixing. Mitochondrial fragmentation (c') was quantified as in (a'). (n=15)

In Fig2d and d', cells were treated with delipidated serum for 24 hours and 30μM mdivi1 for 3 hours. Mitochondrial fragmentation (d') was quantified as in (a'). (n=15)

In Fig. e and e', HeLa cells were seeded into chamber slides and transiently transfected with photoactivatable mitoGFP. After treatment for 24 hours in medium containing delipidated serum, a small region of the mitochondrial network (shown in red using mitotracker) was photoactivated (green) and dispersion of the photoactivated GFP to the rest of the network was monitored for the indicated time points. To quantify the percentage of GFP-positive mitochondria, GFP mitochondrial area was divided by the area of the total

mitochondrial network (red), shown in (e'). The impaired mitochondrial fusion was rescued by treatment with C18:0.

For Fig. 3a, *Drosophila* S2 cells growing in Serum Free Medium (SFM) were treated with either control dsRNA or dsRNA targeting dElovl6. Cells were subsequently transiently transfected +/- HA-tagged dMfn (red) and mitoGFP to visualize mitochondria (green).

In Fig. 3b, *Drosophila* S2 cells growing in SFM were treated with either control dsRNA or dsRNA targeting dMfn, and treated in the absence or presence of C18:0 (100μM) for 2 hours. Mitochondria were visualized with mitoGFP and cell membranes were stained with phalloidin (red).

In Fig. 3 c, to show that ubiquitously expressed dMfn (daughterless-GAL4) fully rescues the lethality of dElovl6 mutant animals until pupation at expected mendelian frequencies, Chi square test was applied ($1.031<3.841=\chi^2$ where $p=0.05$). Flies were grown on antifungal free food at high density. (n=685)

For Fig 3.d, synchronized 1st instar larvae were grown on standard food in the absence or presence of 10% C18:0 for 7 days. Values show the average size of 6 larvae.

In Fig. 3e, HeLas were transfected with non-targeting control siRNA or HUWE1 siRNA for 2 days, then treated with medium containing control or delipidated

serum for 8 hours, and then stimulated either with BSA or BSA loaded with C18:0 (100μM) for 2 hours prior to cell lysis. Endogenous Mfn2 was immunoprecipitated and endogenous ubiquitination was detected with anti-ubiquitin antibody. See Supplementary Information Figure 1 for image of the uncropped full western blot.

In Fig. 3f and f', HeLas were transfected with siRNAs for 2 days, then treated with medium containing normal or delipidated serum 24 hours, and then treated +/- C18:0 for 2 hours prior to imaging the mitochondrial network with mitotracker.

For Fig. 3g and g', HeLa cells were pretreated with the JNK inhibitor SP600125 (10μM) for 30 minutes before incubating cells with medium containing control or delipidated serum for 24 hours. Representative images in (g) and quantification of mitochondrial fragmentation in (g'). (n=15)

In Fig. 3h, HeLa cells transfected with control or TfR1-targeting siRNAs for 2 days, then treated with medium containing normal or delipidated serum for 24 hours, and then treated +/- C18:0 for 2 hours, prior to imaging mitochondrial networks with mitotracker. Quantification of mitochondrial fragmentation is shown in Fig, 3h and representative images are in ED Fig. 7d. (n=15)

For Fig. 3i, TfR1 of HeLa cells were activated with 1μM Gambogic Acid (GA) , that are pretreated with C18:0 or BSA (mock) for 1 hour. Quantification of

mitochondrial fragmentation is shown in Fig. 3i and representative images in ED Fig. 9b. (n=15)

In Fig. 3j, HeLa cells were treated with SP600125 (10μM) 30 minutes prior to 2 hours GA treatment. Quantification of mitochondrial fragmentation is shown in Fig. 3j (n=15) and representative images in ED Fig. 9e.

In Fig.4a and a', control adult female flies were fed with food that is supplemented with 10% C18:0, mitochondrial morphology was visualized with mitoGFP and mitochondrial fragmentation index was calculated as indicated before. (4 animals per condition, 6 optical areas per animal)

In Fig. 4b and b',,36 hours prewandering female control larvae that are expressing mitoGFP were starved on PBS agar for 8 hours. Body wall mitochondria were imaged (b) and mitochondrial fragmentation was quantified (b'). (3 animals per condition, 16 optical areas per animal)

Cell culture, plasmids, transfections and treatments

Drosophila S2 cells were grown in Gibco Serum Free Medium (SFM) supplemented with 20mM L-Glutamine (Gibco), Penicillin (50u/mL) and Streptomycin (50μg/mL) from PAA at 25°C. Cells were tested for negative for mycoplasma contamination.

HeLa cells (ATCC) were cultured in Dulbecco's Modified Eagle Medium supplemented with 10% Bovine Serum (PAA Gold), Penicillin(50u/mL) & Streptomycin(50µg/mL) from PAA. HeLa cells were authenticated by PCR by Multiplexion GmbH. Cells were tested for negative for mycoplasma contamination.

Plasmid transfections were done with Effectene (Qiagen) as per manufacturer's instructions, except PA-mitoGFP which was transfected with Lipofectamine2000 (Life Technologies). To induce expression of genes under transcriptional control of the metallothionine promoter, 700µM $CuSO_4$ was added to the cell culture medium 4 hours after transfection. The following plasmids were used: Myc-Mfn2[53] (addgene #23213) and PA-GFPmt[54] (addgene #19989) were kindly provided by Antonio Zorzano, HA-Ub (addgene #17608), tub>mitoGFP (described in [55]), UAS-dElovl6 (dElovl6 was PCR amplified from cDNA of control flies with oligos listed below containing XbaI and XhoI sites, and cloned into pUAST), pMT-HA-dElovl6 (dElovl6 was PCR amplified from UAS-dElovl6 with oligos listed below, containing EcoRI and BglII restriction sites, and cloned into pMT3b containing an N-terminal HA tag), pMT-dElovl6-HA (dElovl6 was PCR amplified from UAS-dElovl6 with indicated oligos containing KpnI and BamHI restriction enzyme sites and cloned into pMT3b backbone with a C- terminal HA tag), UAS-hElovl6 (hElovl6 was PCR amplified from cDNA of HeLa cells with

oligos listed below, containing BglII and NotI restriction sites, and cloned into pUAST).

dsRNA knockdown was performed by treating the cells with 6ug/mL dsRNA for 7 days for dElovl6 and 5 days for dMfn. dsRNA was synthesized by PCR amplifying the region of the transcript to be targeted with primers containing a T7 promoter and the amplicon was used as the template for *in vitro* transcription reaction with T7 transcriptase (Fermentas). siRNA transfection of HeLa cells were done with Lipofectamine RNAi Max (Life Technologies) as per manufacturer's instructions. siRNAs were purchased from Thermo Scientific Bio and their catalog numbers and sequences were listed in Supplementary Table 1.

Supplementary Table 1: Catalog numbers and sequences of the siRNAs

Gene	**siRNA from Thermo Scientific Bio**	**Sequences**
PINK1	MU-004030-02	GCAAAUGUGCUUCAUCUAA, GGAGCCAUCGCCUAUGAAA, GAGCAUCGGCCUGCAGUUG, GAAAUCCGACAACAUCCUU
PARK2	MU-003603-00	GUAAAGAAGCGUACCAUGA, UUAAAGAGCUCCAUCACUU, UCAAGGAGGUGGUUGCUAA, GGAGUGCAGUGCCGUAUUU

AMFR	MU-006522-01	GCAAGGAUCGAUUUGAAUA, GGAGCUGGCUGUCAACAAU, GAGGACUGCUCAUGUGAUU, CGAGCUGGCUGCCGAGUUU
HUWE1	MU-007185-01	GCAAAGAAAUGGAUAUCAA, GGAAGAGGCUAAAUGUCUA, GAAAUGGAUAUCAAACGUA, UAACAUCAAUUGUCCACUU
MARCH5	MU-007001-01	GACAGAAGUUGCUGGGUUU, GUAAAUUGAUGUUCAGUAG, GGACAGCUGUGACUUAUGG, UCAAACAGCAGCAAUAUUU
TfR1 (TFRC)	MU-003941-02-0002	GGAGAACCAUUGUCAUAUA, GGACACAGAUUAUCCUUAU, GCACAGCUCUCCUAUUGAA, CCACUGUUGUAUACGCUUA
ZDHHC6	MU-014101-01-0002	CAAGUAAGUUAACGGCAUU, CCAUGUAUCUCCAGUAUUG, GGGAUUAGCUUUAGGAACA, GGACUUGAGUGGCCAGUAA
IRE1 (ERN1)	MU-004951-02-0002	CCCAAAAGCCUUACGGUCA, AGAACAAGCUCAACUACUU, GGAAGUACCAGCACAGUGA,

		CCAAGAUGCUGGAGAGAUU
ATF6	MU-009917-01-0002	GAACAGGGCUCAAAUUCUC, AACCAAAUCUGUACAGUUA, UCACACAGCUCCCUAAUCA, GAACAGGAUUCCAGGAGAA
PERK (EIF2AK3)	MU-004883-03-0002	GAAGCUACAUUGUCUAUUU, UAGCAAAUCUUCUUCUGAA, UAAACUAACUGCUUUCAAG, ACUAAUCGAUUGCAUAUUG
LIAS	MU-010023-00-0002	GGAGAAAGGUUAAGACUAC, CAAAGACCGUAUCAUAUUU, UACAAGAGGUUGCAGAUUU, GAGGUGAUCUCAAAGCAAU
SDHB	MU-011773-02-0002	GGUAUUGGAUGCUUUAAUC, GAACAUCAAUGGAGGCAAC, GUGAGAAACUGGACGGGCU, GCUACUGGUGGAACGGAGA
Control (Rluc)	P-002070-01	AAAAACATGCAGAAAATGCTG

Fatty acids were added to cell culture media by first conjugating them to BSA using a protocol adapted from [56]: Fatty acids were dissolved in 0.1M NaOH at 95ºC at 50mM concentration. 100µL of this fatty acid solution was added dropwise onto 600µL 10% fatty acid free BSA (Calbiochem) at 50ºC with

vortexing. 300µL ddH_2O was added to yield a 5mM solution. The same process was repeated without any fatty acid to obtain a BSA solution for mock treatments. Solutions were passed through a 0.45µm filter and added to cell culture media at a dilution of 1:50.

Serum was delipidated as described in [57]. Briefly, 2 volumes of premixed butanol:diisopropyl ether (25:75) was added to 1 volume of serum to be delipidated containing 0.1mg/mL EDTA. The mixture was end-over-end rotated for 3 hours. The mixture was centrifuged 2000rpm for 2 minutes at room temperature and the aqueous layer was carefully saved and degased. For treatments, HeLa cells were grown in DMEM containing this delipidated serum for 24 hours.

10 µM JNK inhibitor SP600125 and the corresponding DMSO mock pretreatments were started 30 mins before delipidated serum treatment.

To prepare cells for electron microscopy, cells were treated with dsRNA for 7 days and fixed in 2% paraformaldehyde, 4% glutaraldehyde (EM grade), 2% sucrose and 10mM phosphate buffer pH 7.5. In order to present the results of EM micrograph analyses, a box plot was generated using the following website: http://boxplot.tyerslab.com/

Cycloheximide (C4859 Sigma) was used at a concentration of 100 µg/mL. The chemical chaperone TUDCA (Calbiochem 580549) was used at a concentration of 500 µg/mL 30 mins prior to treatment with delipidated serum.

C15:0-azide (15-azidopentadecanoic acid) from Life Technologies (C10265).

Fly stocks

The dElovl6^{-} fly line (l(3)02281$^{-/-}$) was a kind gift from Mireille Schäfer [58]. UAS-AOX was a kind gift from Dr. Howy Jacobs [59]. UAS-Spargel was a kind gift from Dr. Cristian Frei [60]. Pink1^{B9}, Pink1^{RV} and Park^{25} lines were originally made by [61] and [62] and kindly provided to us by Patrik Verstreken[63]. Actin-Gal4, daughterless-Gal4 and UAS-HUWE1-RNAi were obtained from the Bloomington Stock Center. Marf/dMfn knockout flies were generated as described previously [63]. To generate the knockout vector, flanking homology regions were amplified using the oligos listed in table below, sequenced, and cloned into pW25.

Fatty acid methyl ester analysis and total fatty acid elongase assay

Lipid extracts were derivatized by acid-catalyzed esterification [64] with 10% BF3 in methanol (Sigma-Aldrich, Gillingham, U.K.), and the esterification was performed at 80°C for 90 min. Once cool, water and hexane were added, and the aqueous layer was discarded. The organic layer was dried and then reconstituted in

hexane for gas chromatography–flame ionization detection analysis (GC-FID) with a Trace GC Ultra (ThermoScientific). Derivatized organic samples were injected onto a 30-m × 0.25-mm 70% cyanopropyl polysilphenylene-siloxane 0.25 µm TR-FAME stationary-phase column (ThermoScientific). The initial column temperature was 55°C for 2 min, increased by 15°C/minute to 150°C and then increased at a rate of 4°C/minute to 230°C, where it was held for 30 s.

Total fatty acid elongation measurement was performed as described in [65].

Survival to pupation assay

Flies were placed to lay eggs in cages on apple juice-agar plates. First-instar larvae hatching within a 12h time window were collected and put into vials containing food at a density of 30 or 60 (indicated in the figure legends) animals per vial. Pupation was then inspected visually.

Life span assay

Larvae were grown at a low density (approximately 100 per bottle). Adults eclosing within a 24 time-window were collected and put into vials containing fly food (10 per vial). Every 2 days the vials were flipped and the number of remaining living animals was recorded. This was repeated until all flies died.

Rotenone sensitivity assay

Rotenone was dissolved in acetone and added into fly food at a final concentration of 100μM. As a mock treatment, only acetone (the vehicle) was added.

Fatty acid supplementation of fly food

Fly food was liquefied by heating and 10% w/w fatty acids were dissolved in it.

ATP measurements

ATP measurements were done by using the Perkin Elmer ATPlite kit (Perkin Elmer 6016941) according to the manufacturer's instructions. 3 adult flies were crushed in 200μl lysis buffer that is provided with the kit.

Fly motility / climbing assay

10 flies were transferred to a transparent tube without being anesthetized. The two tubes containing two fly genotypes to be compared were tapped in parallel a minimum amount of times necessary to bring all flies to the bottom . The number of flies that were able to climb over a certain threshold in a given time period was quantified.

Respiration assay for Elovl6 mutants

6 larvae that are 24 hours pre-wandering were taken out of the food and washed with PBS. Their weight was recorded. They were inverted in ice cold PBS and permeabilized in ice cold 25µM digitonin containing respiration buffer (0.5mM EGTA, 3mM $MgCl_2.6H_2O$, 60mM K-Lactobionate (lactobionic acid is dissolved in H_2O and pH is adjusted to pH 7.4 with KOH), 20mM Taurine, 10mM KH_2PO_4, 20mM HEPES, 110mM sucrose, 1g/L fatty acid free BSA) at 4ºC for 10 minutes by gentle rocking. Larvae were then washed with digitonin-free respiration buffer. Oroboros O2k high resolution respirometry oxygraph chambers were filled with respiration buffer and left to be air calibrated at 25ºC. Larvae were put into the chambers and chambers were closed. Catalase was added at a final concentration of 280u/ml and H_2O_2 was injected into the chambers in small volumes to increase oxygen concentration to around 500µM. After equilibration was achieved, oxygen consumption in the presence of 10mM proline, 10mM pyruvate, 5mM malate, 5mM glutamate and 2mM ADP was measured, which is complex I dependent respiration. Then, 10mM succinate and 15mM glycerol-3-phosphate (final concentrations) were injected into the chamber to induce complex II as well. Non-mitochondrial respiration was measured by inhibiting complex I with rotenone (0.5µM) and complex III with antimycin A (2.5µM).

For measuring complex IV activity, the steps were the same as complex I&II activity measurement until the substrate injections. 0.5 mM TMPD, that could be directly oxidized by complex IV was added in presence of 0.25mM ascorbic acid, which prevents autooxidation of TMPD at oxygen pressure (final concentrations). After the values are recorded, 1 mM KCN was added to the chamber to inhibit complex IV and measure non-mitochondrial oxygen consumption. Protocols were adapted from [66].

All values were corrected for non-mitochondrial oxygen consumption and normalized to wet weight of the larvae. Always 2 sets of samples to be compared were run in parallel in the two chambers of the oxygraph.

Respiration assay on Mfn knockout animals

Larvae (n = 10) 24 hours after hatching were collected, washed with cold PBS and the bodyweight were measured. Then larvae were dissected in cold BIOPS medium (2.77mM CaK_2EGTA, 7.23 mM K_2EGTA, 5.77mM Na_2ATP, 6.56 mM $MgCl_2 \cdot 6H2O$, 20mM Taurine, 15 mM Na_2Phospho-creatine, 20 mM Imidazole, 0.5mM DTT, 50mM MES,pH7.1) supplied with 25 µM digitonin. Inverted larvae were transferred to MITOMED R05 medium (0.5 mM EGTA, 3mM $MgCl_2 \cdot 6H2O$, 60 mM K-lactobionate, 20 mM Taurine, 10mM KH_2PO_4, 20 mM HEPES, 110 mM Sucrose, 1g/L BSA, 25 25µM digitonin pH7.1). The respiratory rate was measured using an oxygraph chamber (OROBOROS) as described previously [67].

Larval bodyweight was used to normalize the oxygen consumption.

Staining of the cells and tissues

Mitotracker staining of the cells was performed in living cells. Mitotracker red (Cell Signaling #9082) was added into the cell culture medium at a final concentration of 50nM, 45 mins prior to fixing.

Cells or freshly dissected larvae in PBS were fixed with 4% methanol free formaldehyde containing PBS for 20 min at room temperature. After rinsing with PBS-0.2% TritonX-100 containing PBS (PBT), cells or larvae were permeabilized in PBT 2x10mins. (If antibody staining will be performed, blocking was performed in PBT containing 0.1% BSA (BBT) for 45 mins. Secondary antibodies conjugated with fluorophores were applied in BBT either for 2 hours at room temperature or at 4ºC overnight.) In the final PBT wash, DAPI and if used, phalloidin, were included. mitoGFP expressing cells or larvae or cells prestained with mitotracker were processed in the dark the whole time. Colocalization coefficient was calculated with Jacop, an Image J plugin [68].

Mitochondrial fragmentation index calculation

The calculation was adapted from [69]. Briefly, by using ImageJ, images were first thresholded and converted to binary images. The particle number was quantified

and divided by the total area of mitochondria, yielding mitochondrial fragmentation index. The fragmentation index was calculated on images in a blinded fashion, without knowing which image corresponded to which sample, and then subsequently 'un-blinded'.

Mitochondrial purification and subsequent fractionation

Purification of mitochondria was performed as described in [70] except that a Dounce homogenizer was used for homogenization. Submitochondrial fractionation was carried out as described in [71].

In vivo mitochondrial fusion assay with live cell imaging

PA-GFPmt (addgene #19989) transfected HeLa cells were imaged with a Leica sp5 confocal microscope with an incubator chamber. A small region of the mitochondrial network was photoactivated with a 405nm laser beam. Time lapse images were acquired with a 7.5 min interval.

Antibodies

Anti-Mfn2 (Cell Signaling #11925), rat anti-HA (Roche, clone 3F10), mouse anti-myc tag (Cell Signaling #2276, clone 9b11), rabbit anti-dMfn (a kind gift from Dr. Alex Whitworth [27]), mouse anti-Ubiquitin (1:500 in BSA/PBS-T, Enzo Lifesciences

FK2), rabbit anti-dPorin (a kind gift from Prof. Dr. Jongkyeong Chung ([72]), mouse anti-ATPsyn-a (abcam - mitosciences 15H4C4), mouse anti-HUWE1 (HECT9 Cell Signaling #5695), mouse anti-Tubulin (Sigma T9026), rabbit anti-Calnexin (ENZO ADI-SPA-860-D), mouse anti-Lamin (1:100 in 5% milk powder/PBS-T, Developmental Studies Hybridoma Bank, ADL 101-s dLamin C), rat anti-Cadherin (1:200 in 5% BSA/PBS-T, Developmental Studies Hybridoma Bank, DCAD2), mouse anti-Actin (1:500 in 5% BSA/PBS-T, Developmental Studies Hybridoma Bank JLA20), rabbit anti cleaved caspase3 (1:500 in 5%BSA/PBS-T, Cell Signalling #9661), anti p-Jun kinase (1:500 in 5%BSA/PBS-T, Cell signaling #9251), anti-TfR1 (Cell signaling #13113), anti-DLAT (PDH E2) (Cell Signaling #12362), anti-OGDH (KGDH E1) (Cell Signaling #13407), anti-SDHB (Mitosciences/Abcam ab14714 1:200 in 5%BSA/PBS-T), anti-Lipoic acid (Abcam ab58724 1:2000 in 5%BSA/PBS-T), anti-NDUFAB1 (Mitosciences/Abcam ab181021 1:2000 in 5%BSA/PBS-T), anti-IBA57 (a kind gift from Prof. Dr. Roland Lill [73] 1:75 in 5%BSA/PBS-T), anti-Transferrin (Santa Cruz sc-393595 1:75 in 5%BSA/PBS-T), p-eIF2α (Cell Signaling #3398). For Western Blotting, antibodies were used at 1:1000 dilution in 5% BSA/PBS-T unless otherwise indicated.

Mfn2 Immunoprecipitation

Lysis of the cells was performed in fully denaturing conditions, both to ensure that post translational modifications are not lost, and to ensure that only the protein of interest is precipitated (ie protein-protein interacts are lost). Cells were

lysed in denaturing lysis buffer (8M urea, 10% glycerol, 10% SDS, 10mM Tris pH 6.8, 200mM DTT). Samples were sonicated with a Bioruptor water bath sonicator for 2.5 minutes at medium strength with 30 seconds on/30 seconds off intervals. Samples were then diluted 1:10 with dilution buffer (10% glycerol, 10mM Tris pH 6.8, 200mM DTT, 10mM N-ethylmaleimide and protease inhibitor cocktail (Roche, 11697498001, 4X final). Before adding antibodies, some of the lysate was spared as an input control. Anti-Mfn2 was used at 1:200 dilution and anti-Myc tag was used at 1:500 dilution.

Syntheses of C16:0-azide, C17:0-azide, C17:0-alkyne, and C18:0-alkyne

Supplementary Figure 1: C16:0-azide synthesis reaction.

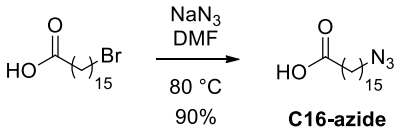

C16:0-azide (16-azidohexadecanoic acid): A mixture of 16-bromohexadecanoic acid (1.000 g, 2.982 mmol, Sigma) and NaN_3 (234.5 mg, 3.617 mmol, Sigma) in DMF (8.0 mL) was submerged in an 80 °C oil bath. After 4.5 h, the mixture was cooled to RT and diluted with H_2O (100 mL) and Et_2O (25 mL). The two layers were separated and the aqueous layer was further extracted with Et_2O (2 x 25 mL). The combined organics were washed with H_2O (3 x 10 mL), brine (10 mL), dried ($MgSO_4$), filtered, and concentrated to give **C16:0-**

azide (801 mg, 90%) as a pure white solid. The analytical data are in accordance with the literature [74,75]. The reaction is presented in Supplementary Figure 1.

R_f 0.34 (5% MeOH in CH_2Cl_2)

mp 47.6–48.0 °C

^{1}H NMR (400 MHz, $CDCl_3$) δ 3.25 (t, *J* = 7.0 Hz, 2 H), 2.34 (t, *J* = 7.5 Hz, 2 H), 1.67–1.56 (m, 4 H), 1.40–1.24 (m, 22 H) ppm.

^{13}C NMR (100 MHz, $CDCl_3$) δ 180.1, 51.7, 34.2, 29.8, 29.8, 29.8, 29.7, 29.7, 29.6, 29.6, 29.4, 29.3, 29.2, 29.0, 26.9, 24.8 ppm.

HRMS-TOF ES (*m/z*): [M+H$^+$] calcd for $C_{16}H_{32}N_3O_2$, 298.2489; found, 298.2499.

Supplementary Figure 2: C17:0-azide synthesis reaction.

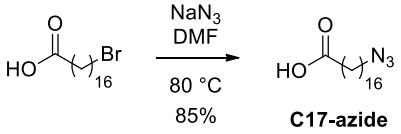

C17:0-azide (17-azidoheptadecanoic acid): A mixture of 17-bromoheptadecanoic acid (250 mg, 0.716 mmol, Fluorochem) and NaN_3 (58.4 mg, 0.898 mmol, Sigma) in DMF (4.0 mL) was submerged in an 80 °C oil bath. After 18 h, the mixture was cooled to RT and diluted with H_2O (100 mL) and Et_2O (25 mL). The two layers were separated and the aqueous layer was further extracted with Et_2O (2 x 25 mL). The combined organics were washed with H_2O (3 x 10 mL), brine (10 mL), dried ($MgSO_4$), filtered, and concentrated to give

C17:0-azide (189 mg, 85%) as a pure white solid. The C17:0-azide synthesis reaction is presented in Supplementary Figure 2.

R_f 0.36 (5% MeOH in CH_2Cl_2)

mp 55.5–56.1 °C

^{1}H NMR (400 MHz, $CDCl_3$) δ 3.25 (t, *J* = 7.0 Hz, 2 H), 2.35 (t, *J* = 7.5 Hz, 2 H), 1.67–1.56 (m, 4 H), 1.40–1.24 (m, 24 H) ppm.

^{13}C NMR (100 MHz, $CDCl_3$) δ 180.1, 51.7, 34.2, 29.8, 29.8, 29.8, 29.8, 29.7, 29.7, 29.6, 29.6, 29.4, 29.3, 29.2, 29.0, 26.9, 24.8 ppm.

HRMS-TOF ES (*m/z*): [M+H$^+$] calcd for $C_{17}H_{34}N_3O_2$, 312.2646; found, 312.2610.

C17:0-alkyne and **C18:0-alkyne** were synthesized following the protocol of Breit [76]. The C17:0-alkyne synthesis reaction and its intermediates is presented in Supplementary Figure 3.

Supplementary Figure 3: C17:0-alkyne synthesis reaction.

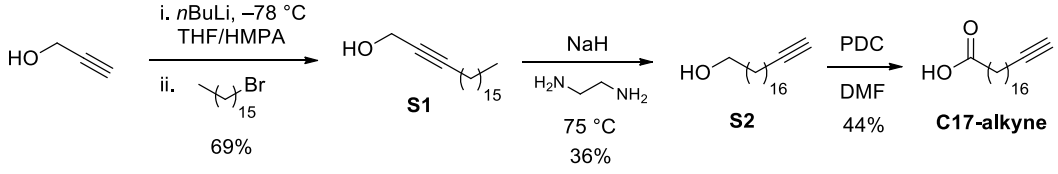

nonadec-2-yn-1-ol (S1): To a solution of freshly distilled (from K_2CO_3) propargyl alcohol (3.35 mL, 57.5 mmol) in THF/HMPA (90 mL/24 mL) was added *n*BuLi (46 mL, 115 mmol, 2.5 M in hexane) dropwise via syringe pump over 35 minutes at

–78 °C under argon. After the addition was complete, the reaction was warmed to –30 °C and 1-bromoheptadecane (13.5 mL, 44.2 mmol) was added dropwise over 8 min via syringe pump. After the addition was complete, the mixture was allowed to warm to RT and stirred overnight. The reaction was quenched with sat'd NH_4Cl (300 mL) and the resulting mixture was extracted with EtOAc (2 x 100 mL). The combined organics were washed with brine (50 mL), dried ($MgSO_4$), filtered, concentrated, and purified by column chromatography (10–30% EtOAc in petroleum ether) to give 8.617 g (69%) of **S1** as a beige solid. The analytical data were identical to the literature.

nonadec-18-yn-1-ol (S2): To ethylenediamine (20.8 mL, 311 mmol) was added NaH (2.35 g, 58.7 mmol, 60% in oil) at 0 °C under argon. The mixture was warmed to RT for 2 h to give a purple mixture that was then heated to 60 °C for 1 h. The greenish mixture was cooled to 40 °C, **S1** (3.99 g, 14.2 mmol) was added, and the resulting mixture was heated to 75 °C for 80 min. The mixture was cooled to 0 °C and quenched by the dropwise addition of H_2O (30 mL) and then 1 M HCl (30 mL). This was diluted further with 1M HCl (100 mL) and Et_2O (100 mL). The two layers were separated and the aqueous layer was extracted with Et_2O (2 x 50 mL). The combined organics were washed with 1 M HCl (120 mL), brine (50 mL), dried ($MgSO_4$), filtered, concentrated, and purified by column chromatography (10–30% EtOAc in petroleum ether) to give 1.91 g of **S2** as a beige solid which contained ~135 mol% EtOAc to give an estimated yield of (36%). The analytical data were identical to the literature.

C17:0-alkyne (nonadec-18-ynoic acid): To a solution of **S2** (867 mg, ~2.4 mmol, ~75% pure) in anhydrous DMF (10 mL) was added pyridinium dichromate (2.655 g, 7.057 mmol) at RT under argon. After 16 h, the reaction was quenched with 1 M HCl (10 mL) and diluted with EtOAc (20 mL). The two layers were separated and the aqueous layer was extracted with EtOAc (2 x 20 mL). The combined organics were washed with brine (20 mL), dried ($MgSO_4$), filtered, and purified by column chromatography (20% EtOAc in petroleum ether) to give 307 mg (~44%) of **C17:0-alkyne** as a white solid. The analytical data were identical to the literature.

Supplementary Figure 4: C18:0-alkyne synthesis reaction.

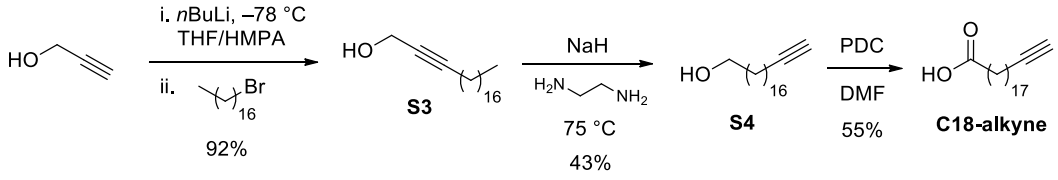

icos-2-yn-1-ol (S3): An identical procedure as for **S1** was followed using propargyl alcohol (1.18 mL, 20.3 mmol), THF/HMPA (33 mL/8.5 mL), *n*BuLi (16.5 mL, 41.2 mmol, 2.5 M in hexanes), and 1-bromoheptadecane (4.96 g, 15.53 mmol) to give 4.21 g (92%) of **S3** as a white solid:

R_f 0.46 (20% EtOAc in petroleum ether)

^{1}H NMR (400 MHz, $CDCl_3$) δ 4.25 (t, *J* = 2.2 Hz, 2 H), 2.21 (tt, *J* = 7.2, 2.2 Hz, 2 H), 1.55–1.45 (m, 3 H), 1.41–1.33 (m, 2 H), 1.32–1.23 (m, 26 H), 0.88 (t, *J* = 6.8 Hz, 3 H) ppm.

icos-19-yn-1-ol (S4): An identical procedure as for **S2** was followed using ethylenediamine (9.8 mL, 147 mmol), NaH (1.63 g, 40.7 mmol), and **S3** (2.00 g, 6.79 mmol) to give 870 mg (43%) of **S4** as a white solid:

R_f 0.39 (20% EtOAc in petroleum ether)

^{1}H NMR (400 MHz, $CDCl_3$) δ 3.64 (t, *J* = 6.6 Hz, 2 H), 2.18 (td, *J* = 7.1, 2.7 Hz, 2 H), 1.93 (t, *J* = 2.7 Hz, 1 H), 1.60–1.48 (m, 4 H), 1.42–1.24 (m, 28 H) ppm.

C18:0-alkyne (icos-19-ynoic acid): An identical procedure as for **C17:0-alkyne** was followed using **S4** (865 mg, 2.94 mmol), PDC (3.32 g, 8.82 mmol), and anhydrous DMF (10 mL) to give 504 mg (55%) of **C18:0-alkyne** as a white solid (The C18:0-alkyne synthesis reaction is presented in Supplementary Figure 4.)

:

R_f 0.31 (20% EtOAc in petroleum ether)

mp 66.6–69.6 °C

^{1}H NMR (400 MHz, $CDCl_3$) δ 2.34 (t, *J* = 7.5 Hz, 2 H), 2.18 (td, *J* = 7.1, 2.7 Hz, 2 H), 1.93 (t, *J* = 2.7 Hz, 1 H), 1.67–1.59 (m, 2 H), 1.56–1.48 (m, 2 H), 1.42–1.22 (m, 26 H) ppm.

^{13}C NMR (100 MHz, $CDCl_3$) δ 179.9, 85.0, 68.2, 34.1, 29.8, 29.8, 29.8, 29.8, 29.8, 29.7, 29.7, 29.6, 29.6, 29.4, 29.3, 29.2, 28.9, 28.6, 24.8, 18.5 ppm.

HRMS-TOF ES (*m/z*): [M-H$^+$] calcd for $C_{20}H_{35}O_2$, 307.2643; found, 307.2640.

NMR spectra of C16:0-azide, C17:0-azide, C17:0-alkyne, and C18:0-alkyne:

NMR spectra to confirm purity of C16:0-azide (Supplementary Figures 5 and 6), C17:0-azide (Supplementary Figures 7 and 8), C17:0-alkyne (Supplementary Figure 9) and C18:0-alkyne (Supplementary Figures 10 and 11) are shown below.

Supplementary Figure 5: NMR spectrum of C16:0-azide.

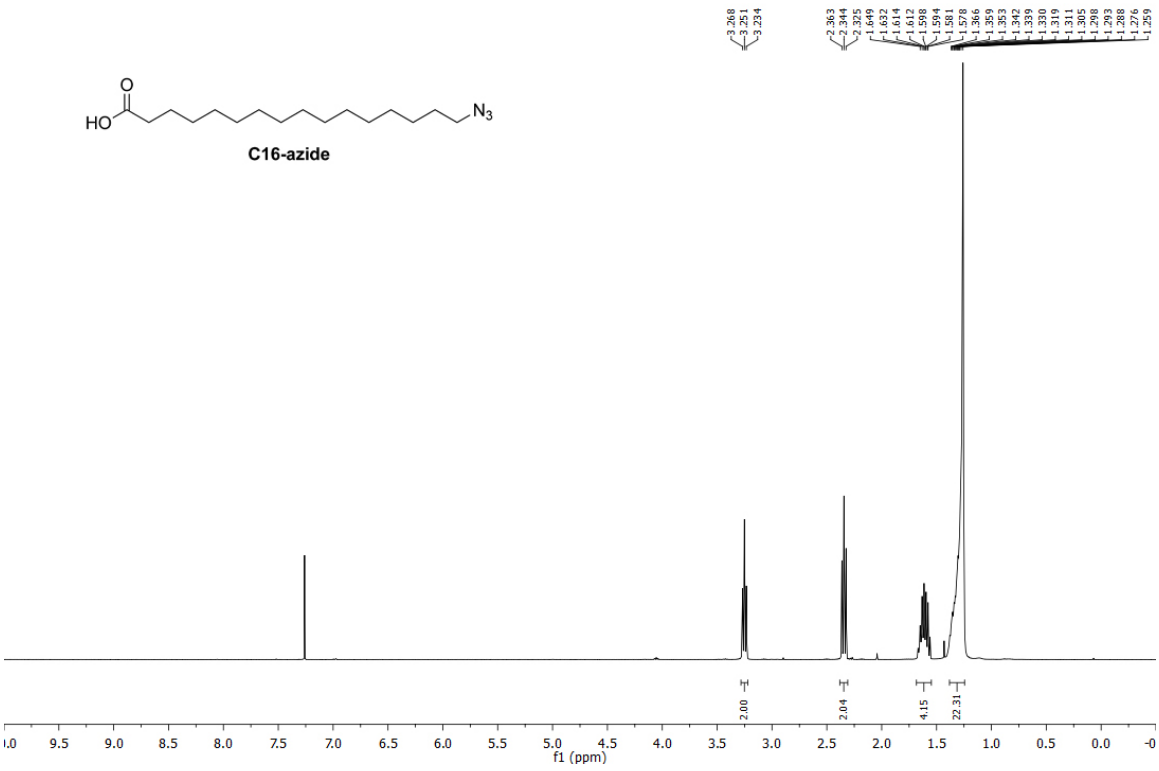

Supplementary Figure 6: NMR spectrum of C16:0-azide.

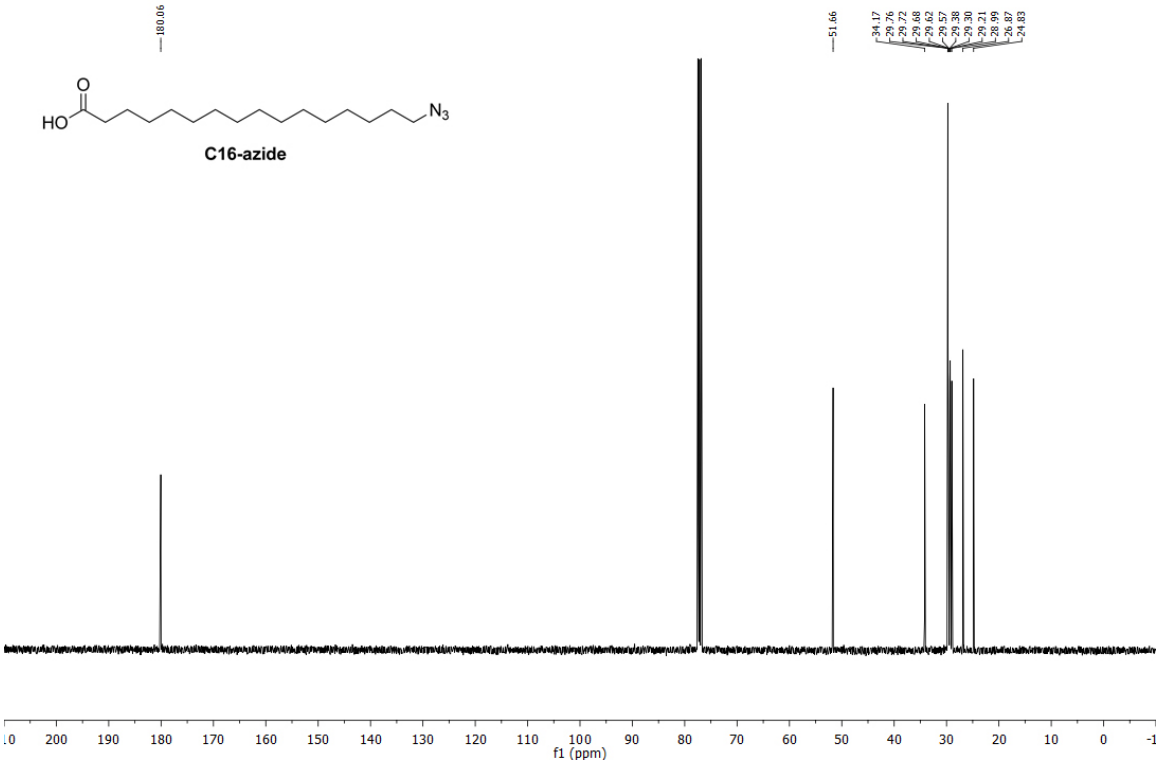

Supplementary Figure 7: NMR spectrum of C17:0-azide.

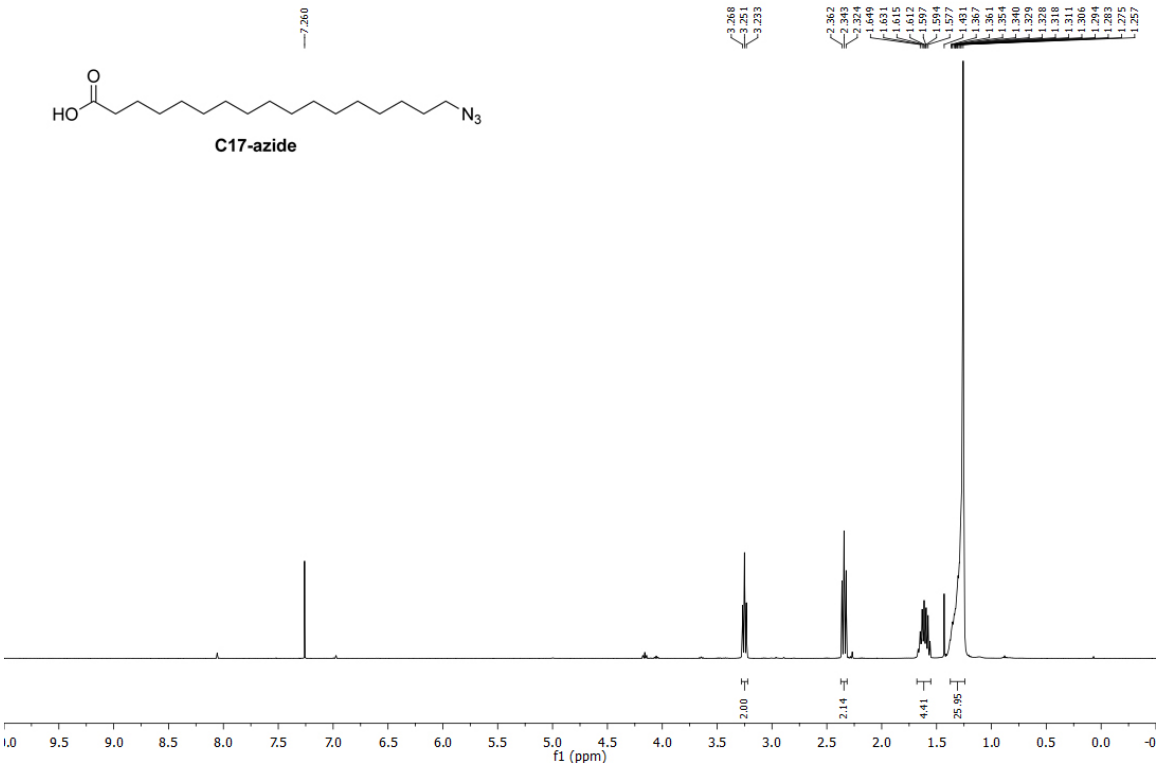

Supplementary Figure 8: NMR spectrum of C17:0-azide.

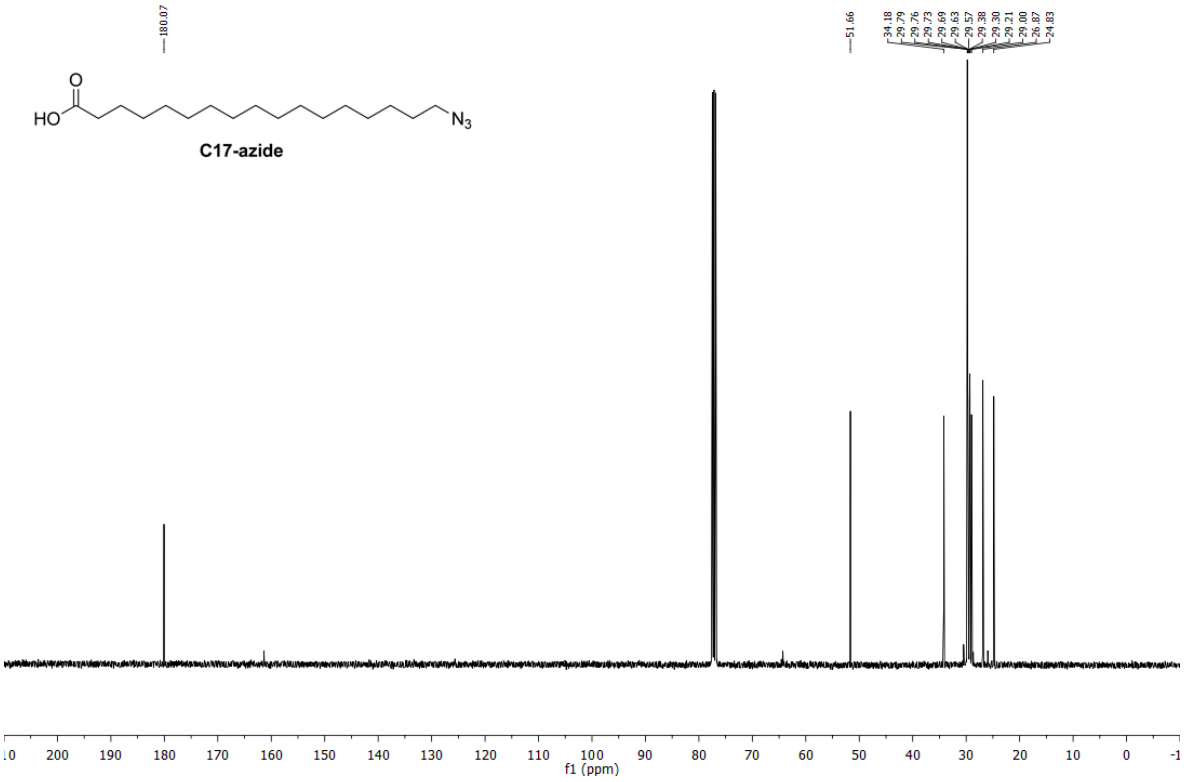

Supplementary Figure 9: NMR spectrum of C17:0-alkyne.

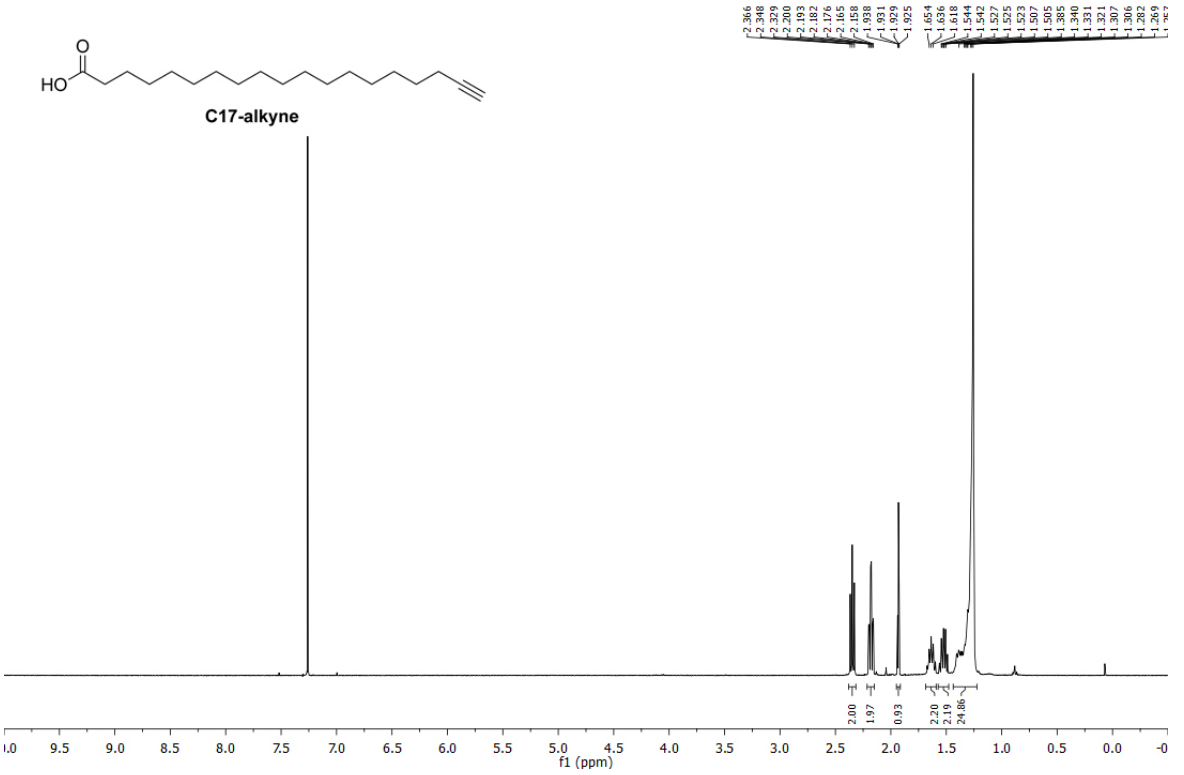

Supplementary Figure 10: NMR spectrum of C18:0-alkyne.

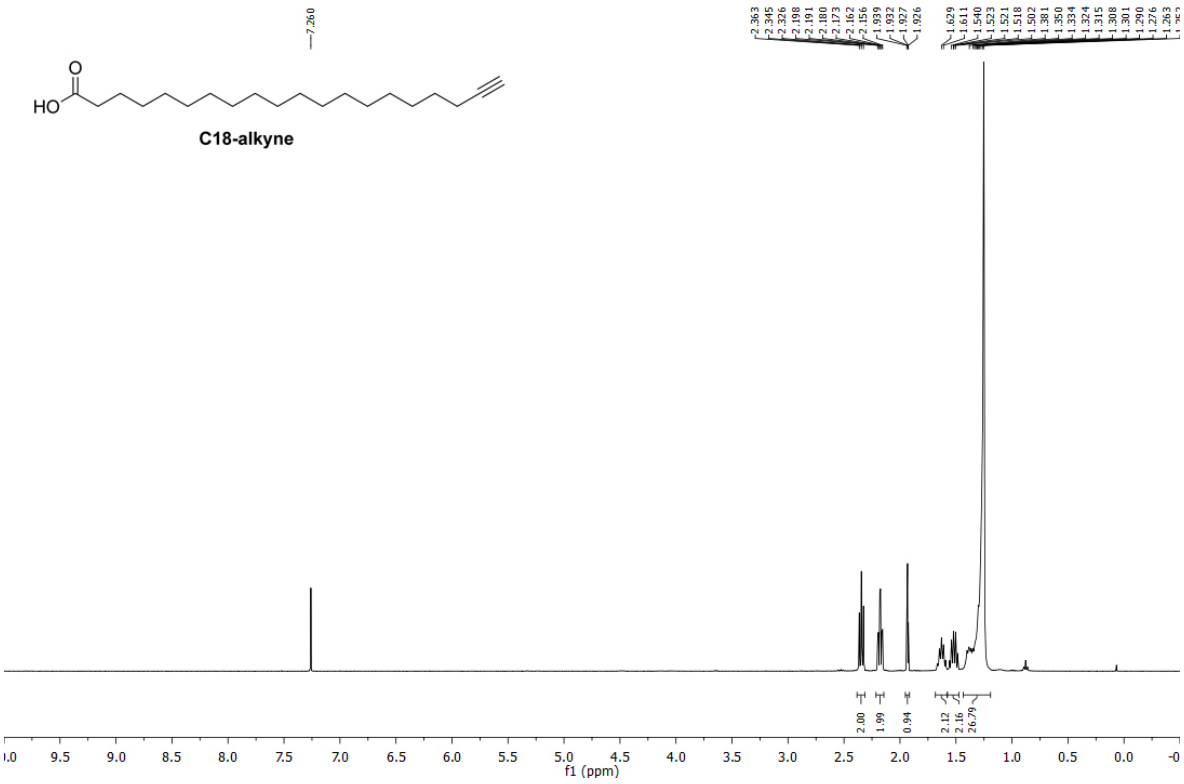

Supplementary Figure 11: NMR spectrum of C18:0-alkyne.

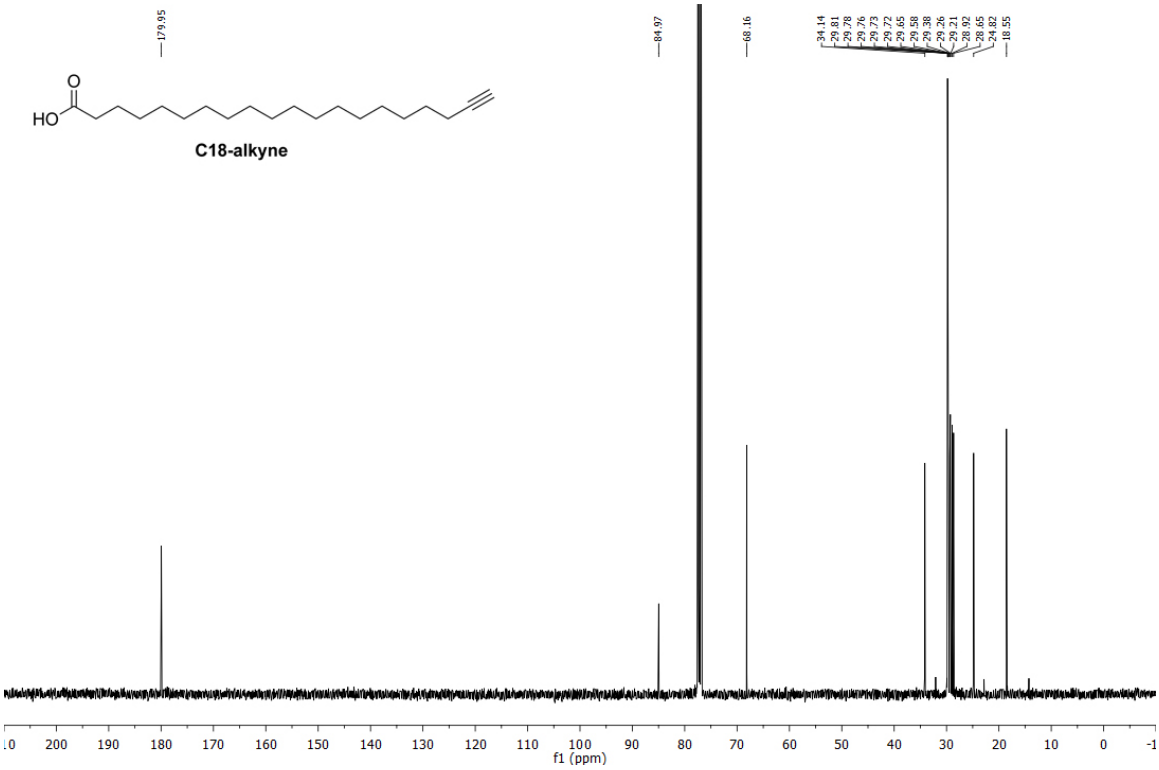

Enrichment of C17:0-azide modified proteins for mass spec analysis

C17:0-azide modified proteins were enriched by using the 'Click-iT protein enrichment kit' from Life Technologies (C10416) as per manufacturer's instructions: Briefly, HeLa cells were seeded in 6 well format at 200,000 cells/well. After overnight adherence of the cells, medium was replaced with medium containing delipidated serum. After 24 hours, cells were incubated with C17:0-azide loaded on BSA (as for C18:0, see "*Cell culture, plasmids, transfections and treatments"* above) for 2 hours. Then, cells were washed twice with PBS to remove unbound C17:0-azide and scraped into PBS. The cell suspension was centrifuged at 4000 rpm for 2 min. Cell pellets were lysed under denaturing conditions in 850 µL urea lysis buffer (8M urea, 2% CHAPS, 1.5M NaCl, 4X final Roche protease inhibitor cocktail, 100 U/mL benzonase (novagen 70746)). Lysates were cleared by centrifuging at 14000 rpm for 10 minutes. 1mL per reaction of 2X catalyst solution was prepared as follows: 835 µL ddH_2O, 125 µL reaction additive 2 (component E) and 20 µL 100 mM Copper (II) sulfate (component E) were mixed and vortexed. Then 20 µL reaction additive 2 (component F) was added to the mixture and it was vortexed again. The Click-iT® reaction was set up in 2mL tubes by adding 800 µL lysate and 1 mL 2X catalyst solution to 200 µL ddH_2O-washed alkyne resin slurry. The mixture was end-over-end rotated overnight. The next day, tubes were centrifuged at 1000 rcf for 1 min to precipitate the resin alkyne slurry. Resin slurry was washed with water and 2%

SDS wash buffer. Samples were then reduced with 10 mM DTT in 1 mL SDS wash buffer at 70°C for 15 mins, after which they were cooled down to room temperature for 15 mins and alkylated with 40 mM iodoacetemine in SDS wash buffer for 30 mins in the dark at room temperature. The resin was then transferred to columns and washed stringently on a vacuum flow with 5X SDS wash buffer, 10X 8M urea / 100mM Tris pH8 and 10X 20% acetonitrile. After that proteins that are bound to resin were digested with 2 µg/mL trypsin (promega sequencing grade) in digestion buffer (100mM Tris, 2mM $CaCl_2$, 10%acetonitrile) at 37°C overnight. Peptides that came off of the beads upon digested were analyzed with a mass spectrophotometer and enriched proteins were identified.

Pulldown of C15:0-azide and C17:0-azide modified proteins

The procedure performed was identical to the enrichment protocol described above, up to the reaction set up. Proteins bound to C15:0-azide and C17:0-azide were labeled with alkyne-biotin by using the 'Click-iT protein reaction buffer kit' (Life Technologies C10276) as per manufacturer's instructions. The Click-iT® reaction was set up as following: in a 1.5 mL tube, 50 µL lysate, 40 µM biotin alkyne (B10185 Life Technologies) containing 100 µL component A (reaction buffer) and 10 µL ddH_2O were added and the tube was vortexed 5''. 10 µL Component B (40 mM Copper (II) sulfate was added and the tube was vortexed 5''. 10 µL of Component C (Reaction additive 1) was added and the tube was vortexed 5". The tube was incubated at room temperature for 2 mins. 20 µL

Component D (Reaction additive 2) was added. The tube was rotated end-over-end for 20 mins. Later, 600 µL methanol was added to the tubes, the tubes were vortexed, 150 µL chloroform was added, the tube was vortexed, 450 µL ddH_2O was added and the tube was vortexed. The tubes were centrifuged at 14000 rpm for 5 mins. Supernatant was discarded. Protein pellet was washed with 450 µL methanol 2 times. Remaining residual methanol was evaporated off on a heat block for 30" and the protein pellet was resuspended in 1% SDS, 30 mM Tris pH8, Roche protease inhibitor cocktail. The resuspension was diluted 1:10 in 50 mM Tris pH 7.5, 150 mM NaCl, Roche protease inhibitor cocktail. 10% of the protein solution was kept aside as 'input'. Biotinylated proteins were pulled down with streptavidin coupled beads (Life Technologies 65001 Dynabeads® MyOne™ Streptavidin C1) overnight at 4°C by end-over-end rotation. The beads were washed 2 times with wash buffer 1 (2% SDS in ddH_2O), wash buffer 2 (0.1% deoxycholate, 1% Triton X-100, 500 mM NaCl, 1 mM EDTA, 50 mM Hepes, pH 7.5), wash buffer 3 (250 mM LiCl, 0.5 M NP-40, 0.5% deoxycholate, 1 mM EDTA, 10 mM Tris pH 8.1) and wash buffer 4 (50 mM Tris pH 7.4, 50 mM NaCl). Biotin labeled proteins were eluted off of the beads with 1mM biotin containing 2X Laemmli buffer (15 mins at room temperature, then 15 mins at 95°C). Eluates were analyzed by western blotting.

Transferrin uptake assay

Live HeLa cells were treated with 25 µg/mL alexa fluor 488 conjugated transferrin (Life Technologies T13342) 30 mins at 37°C prior to fixing.

Tricine SDS-PAGE for small molecular weight proteins

To perform immunoblotting anti-NDUFAB1, we separated proteins by tricine SDS-PAGE, adapting a protocol from Schägger, 2006 [77]. Briefly, cells were lysed in 3% SDS, 1.5% mercaptoethanol, 7.5% glycerol, 0.05% Coomassie blue, 37.5mM Tris pH 7.0 and incubated at 37°C for 1h. Proteins were resolved on a 16% acrylamide (acrylamide : bisacrylamide = 19:1) / 6M urea gel. Proteins were transferred with a semi-dry blotter overnight in transfer buffer (300mM Tris, 100mM acetic acid, pH8.6) at 15V, 0.4mA/cm^2 membrane.

PDH, KGDH and SDH enzyme activity assays

Colorimetric assay kits from Biovision were used for all enzyme activities as per manufacturer's instructions. For all assays, roughly 10^6 cells were lysed in 100 µL respective assay buffers for 10 min on ice. For PDH and KGDH assays, protein precipitations was performed to reduce background by adding 2 fold volume of saturated (~4.1M) ammounium sulfate solution, vortexing, incubating 20 mins on ice and pelleting the protein precipitate by centrifuging at 4°C, 14000 rpm for 5 mins. The pellet was resuspended in the starting volume of respective assay buffer. 20 µL lysate per well was used for all the assays.

Citrate synthase activity assay

3 larvae were homogenized in 200µL lysis buffer (0.25% Triton X/PBS). Lysate was further diluted 1:2 in lysis buffer. 40µL of diluted lysate of each condition was used for measurement in 96 well plate format by adding 60µL reaction buffer to a final concentration of 0.25% Triton X-100, 0.31mM acetyl CoA, 0.1mM DNTB and 0.5mM oxaloacetate. Absorbance was measured at 412nm at 30°C over time and the slope of the curve was used to determine activity.

Statistics and Data Analysis

Sample size selection: For Drosophila phenotypic analyses, we always perform biological triplicates, with 30-60 animals per sample for visual phenotypes (e.g. survival) and 5-10 animals per sample for molecular phenotypes (e.g. oxygen consumption, ATP measurement) to assure the measurement is within linear range of the molecular assay. For cell phenotyping (e.g. mitochondrial fragmentation) we imaged 3-5 microscope fields, each containing 3-5 transfected cells (e.g. mito-GFP), except figure 2b where we used 50 cells in total per condition. All analyses of mitochondrial fragmentation were performed in a blinded fashion as follows. Microscope slides containing cells were prepared by D.S. A colleague was then asked to label the slides with code numbers. Only after D.S. imaged the slides on the confocal, quantified mitochondrial

fragmentation, and performed the statistical analyses, was the identity of each sample revealed. No data or animals/cells were excluded from any data analysis. Student t-tests were used to assess statistical significance, except for Figure 2b-b' because the data are non-parametric.

Oligos

Purposes and sequences of the oligos that were used are listed in Supplementary Table 2.

Supplementary Table 2: Purposes and sequences of the oligos used.

Purpose		**Sequence**
pUAST-dElovl6 construction	F	gggCTCGAGATGATCAACATGGACATT
	R	gggTCTAGATTACTGCGCCTTGGCCTT
PMT-HA-dElovl6 construction	F	gggGAATTCATGATCAACATGGACATT
	R	gggAGATCTTTACTGCGCCTTGGCCTT
PMT-HA-dElovl6 construction	F	gaaGGTACCATGATCAACATGGACATT
	R	gaaGGATCCCTGCGCCTTGGCCTTG
pUAST-hElovl6 construction	F	ggccagatctATGAACATGTCAGTGTTGACTT
	R	ggccgcggccgcTGGCTTCCTCCTCAGTTCCAAC
dsRNA synthesis, control (against luciferase)	F	taatacgactcactatagggAAATGTCCGTTCGGTTGG

	R	taatacgactcactatagggCGAGAATCTCACGCAGGC
dsRNA synthesis,dElovl6	F	taatacgactcactatagggAAGCGGGCCGCCTTC
	R	taatacgactcactatagggTCACCACATCACCGTGCT
dsRNA synthesis, dMfn	F	TAATACGACTCACTATAGGGTGCAGGTTACGCGGGAAATGAAGAT
	R	TAATACGACTCACTATAGGGCCAATACTGCTCTGTCGATTGACCA
mitofusin (Marf) knockout - upstream flank	F	ccgggcggccgcGCAAAGCAGCCACTGTCAA
mitofusin (Marf) knockout - upstream flank	R	ccgggcggccgcGCGTGCAGGGCTGAAAGAG
mitofusin (Marf) knockout - downstream flank	F	ccggggcgcgccGGCGGCCCCTTTAGTTAGT
mitofusin (Marf) knockout - downstream flank	R	ccggggcgcgccGCCTGAGTCCCGAGATCAT
qPCR PERK	F	TCATCCAGCCTTAGCAAACC
qPCR PERK	R	ATGCTTTCACGGTCTTGGTC
qPCR BiP	F	CACAGTGGTGCCTACCAAGA
qPCR BiP	R	TGTCTTTTGTCAGGGGTCTTT
qPCR CHOP	F	AGCCAAAATCAGAGCTGGAA
qPCR CHOP	R	TGGATCAGTCTGGAAAAGCA
qPCR ATF4	F	GTCCCTCCAACAACAGCAAG
qPCR ATF4	R	CTATACCCAACAGGGCATCC
qPCR Marf	F	GCGGTGTCCTCCATTGGAT
qPCR Marf	R	ACGCCAGCCGATAGTTTTCA
qPCR TfR1	F	CTGCTTTCCCTTTCCTTGCATATT
qPCR TfR1	R	GCTCGTGCCACTTTGTTCAACT
qPCR HIF2α	F	AATCAGCTTCCTGCGAACACA

qPCR HIF2α	R	GGTCACCACGGCAATGAAAC
qPCR Ferritin H	F	CCATCAACCGCCAGATCAA
qPCR Ferritin H	R	TCGTTGGTTCTGCAGCTTCA
qPCR hRpl19	F	ATGTATCACAGCCTGTACCTG
qPCR hRpl19	R	TTCTTGGTCTCTTCCTCCTTG

3. References for Supplementary Materials & Methods

1 Jakobsson, A., Westerberg, R. & Jacobsson, A. Fatty acid elongases in mammals: their regulation and roles in metabolism. *Progress in lipid research* **45**, 237-249, doi:10.1016/j.plipres.2006.01.004 (2006).

2 Guillou, H., Zadravec, D., Martin, P. G. & Jacobsson, A. The key roles of elongases and desaturases in mammalian fatty acid metabolism: Insights from transgenic mice. *Progress in lipid research* **49**, 186-199, doi:10.1016/j.plipres.2009.12.002 (2010).

3 Moon, Y. A., Shah, N. A., Mohapatra, S., Warrington, J. A. & Horton, J. D. Identification of a mammalian long chain fatty acyl elongase regulated by sterol regulatory element-binding proteins. *The Journal of biological chemistry* **276**, 45358-45366, doi:10.1074/jbc.M108413200 (2001).

4 Green, C. D., Ozguden-Akkoc, C. G., Wang, Y., Jump, D. B. & Olson, L. K. Role of fatty acid elongases in determination of de novo synthesized monounsaturated fatty acid species. *Journal of lipid research* **51**, 1871-1877, doi:10.1194/jlr.M004747 (2010).

5 Matsuzaka, T. *et al.* Cloning and characterization of a mammalian fatty acyl-CoA elongase as a lipogenic enzyme regulated by SREBPs. *Journal of lipid research* **43**, 911-920 (2002).

6 Matsuzaka, T. *et al.* Crucial role of a long-chain fatty acid elongase, Elovl6, in obesity-induced insulin resistance. *Nature medicine* **13**, 1193-1202, doi:10.1038/nm1662 (2007).

7 Wang, Y. *et al.* Elevated hepatic fatty acid elongase-5 activity affects multiple pathways controlling hepatic lipid and carbohydrate composition. *Journal of lipid research* **49**, 1538-1552, doi:10.1194/jlr.M800123-JLR200 (2008).

8 Moon, Y. A., Hammer, R. E. & Horton, J. D. Deletion of ELOVL5 leads to fatty liver through activation of SREBP-1c in mice. *Journal of lipid research* **50**, 412-423, doi:10.1194/jlr.M800383-JLR200 (2009).

9 Zadravec, D. *et al.* Ablation of the very-long-chain fatty acid elongase ELOVL3 in mice leads to constrained lipid storage and resistance to diet-induced obesity. *FASEB journal : official publication of the Federation of American Societies for Experimental Biology* **24**, 4366-4377, doi:10.1096/fj.09-152298 (2010).

10 Moon, Y. A., Ochoa, C. R., Mitsche, M. A., Hammer, R. E. & Horton, J. D. Deletion of ELOVL6 Blocks the Synthesis of Oleic Acid but does not Prevent the Development of Fatty Liver or Insulin Resistance. *Journal of lipid research*, doi:10.1194/jlr.M054353 (2014).

11 Matsuzaka, T. *et al.* Elovl6 promotes nonalcoholic steatohepatitis. *Hepatology* **56**, 2199-2208, doi:10.1002/hep.25932 (2012).

12 Shimano, H. Novel qualitative aspects of tissue fatty acids related to metabolic regulation: lessons from Elovl6 knockout. *Progress in lipid research* **51**, 267-271, doi:10.1016/j.plipres.2011.12.004 (2012).

13 Tang, N. *et al.* Ablation of Elovl6 protects pancreatic islets from high-fat diet-induced impairment of insulin secretion. *Biochemical and biophysical research communications* **450**, 318-323, doi:10.1016/j.bbrc.2014.05.113 (2014).

14 Matsuzaka, T. & Shimano, H. Elovl6: a new player in fatty acid metabolism and insulin sensitivity. *Journal of molecular medicine* **87**, 379-384, doi:10.1007/s00109-009-0449-0 (2009).

15 Liu, Y. *et al.* Genetic analysis of the ELOVL6 gene polymorphism associated with type 2 diabetes mellitus. *Brazilian journal of medical and biological research = Revista brasileira de pesquisas medicas e biologicas / Sociedade Brasileira de Biofisica ... [et al.]* **46**, 623-628, doi:10.1590/1414-431X20133103 (2013).

16 Morcillo, S. *et al.* ELOVL6 genetic variation is related to insulin sensitivity: a new candidate gene in energy metabolism. *PloS one* **6**, e21198, doi:10.1371/journal.pone.0021198 (2011).

17 Wang, Y. *et al.* Regulation of hepatic fatty acid elongase and desaturase expression in diabetes and obesity. *Journal of lipid research* **47**, 2028-2041, doi:10.1194/jlr.M600177-JLR200 (2006).

18 Zorzano, A., Liesa, M. & Palacin, M. Mitochondrial dynamics as a bridge between mitochondrial dysfunction and insulin resistance. *Archives of physiology and biochemistry* **115**, 1-12, doi:10.1080/13813450802676335 (2009).

19 Ohno, Y. *et al.* ELOVL1 production of C24 acyl-CoAs is linked to C24 sphingolipid synthesis. *Proceedings of the National Academy of Sciences of the United States of America* **107**, 18439-18444, doi:10.1073/pnas.1005572107 (2010).

20 Naon, D. & Scorrano, L. At the right distance: ER-mitochondria juxtaposition in cell life and death. *Biochimica et biophysica acta* **1843**, 2184-2194, doi:10.1016/j.bbamcr.2014.05.011 (2014).

21 Bockler, S. & Westermann, B. ER-mitochondria contacts as sites of mitophagosome formation. *Autophagy* **10**, 1346-1347, doi:10.4161/auto.28981 (2014).

22 Poole, A. C. *et al.* The PINK1/Parkin pathway regulates mitochondrial morphology. *Proceedings of the National Academy of Sciences of the United States of America* **105**, 1638-1643, doi:10.1073/pnas.0709336105 (2008).

23 Yang, Y. *et al.* Pink1 regulates mitochondrial dynamics through interaction with the fission/fusion machinery. *Proceedings of the National Academy of Sciences of the United States of America* **105**, 7070-7075, doi:10.1073/pnas.0711845105 (2008).

24 Park, J., Lee, G. & Chung, J. The PINK1-Parkin pathway is involved in the regulation of mitochondrial remodeling process. *Biochemical and biophysical research communications* **378**, 518-523, doi:10.1016/j.bbrc.2008.11.086 (2009).

25 Deng, H., Dodson, M. W., Huang, H. & Guo, M. The Parkinson's disease genes pink1 and parkin promote mitochondrial fission and/or inhibit fusion in Drosophila. *Proceedings of the National Academy of Sciences of the United States of America* **105**, 14503-14508, doi:10.1073/pnas.0803998105 (2008).

26 Poole, A. C., Thomas, R. E., Yu, S., Vincow, E. S. & Pallanck, L. The mitochondrial fusion-promoting factor mitofusin is a substrate of the PINK1/parkin pathway. *PloS one* **5**, e10054, doi:10.1371/journal.pone.0010054 (2010).

27 Ziviani, E., Tao, R. N. & Whitworth, A. J. Drosophila parkin requires PINK1 for mitochondrial translocation and ubiquitinates mitofusin. *Proceedings of the National Academy of Sciences of the United States of America* **107**, 5018-5023, doi:10.1073/pnas.0913485107 (2010).

28 Cha, G. H. *et al.* Parkin negatively regulates JNK pathway in the dopaminergic neurons of Drosophila. *Proceedings of the National Academy of Sciences of the United States of America* **102**, 10345-10350, doi:10.1073/pnas.0500346102 (2005).

29 Kurokawa, M. *et al.* A network of substrates of the E3 ubiquitin ligases MDM2 and HUWE1 control apoptosis independently of p53. *Science signaling* **6**, ra32, doi:10.1126/scisignal.2003741 (2013).

30 Vandewalle, J. *et al.* Ubiquitin ligase HUWE1 regulates axon branching through the Wnt/beta-catenin pathway in a Drosophila model for intellectual disability. *PloS one* **8**, e81791, doi:10.1371/journal.pone.0081791 (2013).

31 Batistic, O., Sorek, N., Schultke, S., Yalovsky, S. & Kudla, J. Dual fatty acyl modification determines the localization and plasma membrane targeting of CBL/CIPK Ca2+ signaling complexes in Arabidopsis. *The Plant cell* **20**, 1346-1362, doi:10.1105/tpc.108.058123 (2008).

32 Veit, M., Reverey, H. & Schmidt, M. F. Cytoplasmic tail length influences fatty acid selection for acylation of viral glycoproteins. *The Biochemical journal* **318 (Pt 1)**, 163-172 (1996).

33 Veit, M., Herrler, G., Schmidt, M. F., Rott, R. & Klenk, H. D. The hemagglutinating glycoproteins of influenza B and C viruses are acylated with different fatty acids. *Virology* **177**, 807-811 (1990).

34 Liang, X. *et al.* Heterogeneous fatty acylation of Src family kinases with polyunsaturated fatty acids regulates raft localization and signal transduction. *The Journal of biological chemistry* **276**, 30987-30994, doi:10.1074/jbc.M104018200 (2001).

35 Fujimoto, T. *et al.* P-selectin is acylated with palmitic acid and stearic acid at cysteine 766 through a thioester linkage. *The Journal of biological chemistry* **268**, 11394-11400 (1993).

36 Bach, R., Konigsberg, W. H. & Nemerson, Y. Human tissue factor contains thioester-linked palmitate and stearate on the cytoplasmic half-cystine. *Biochemistry* **27**, 4227-4231 (1988).

37 Jian, J., Yang, Q. & Huang, X. Src regulates Tyr(20) phosphorylation of transferrin receptor-1 and potentiates breast cancer cell survival. *The Journal of biological chemistry* **286**, 35708-35715, doi:10.1074/jbc.M111.271585 (2011).

38 Kasibhatla, S. *et al.* A role for transferrin receptor in triggering apoptosis when targeted with gambogic acid. *Proceedings of the National Academy of Sciences of the United States of America* **102**, 12095-12100, doi:10.1073/pnas.0406731102 (2005).

39 Zhu, X. *et al.* Mechanisms of gambogic acid-induced apoptosis in non-small cell lung cancer cells in relation to transferrin receptors. *Journal of chemotherapy* **21**, 666-672, doi:10.1179/joc.2009.21.6.666 (2009).

40 Ortiz-Sanchez, E. *et al.* Enhanced cytotoxicity of an anti-transferrin receptor IgG3-avidin fusion protein in combination with gambogic acid against human malignant hematopoietic cells: functional relevance of iron, the receptor, and reactive oxygen species. *Leukemia* **23**, 59-70, doi:10.1038/leu.2008.270 (2009).

41 Pandey, M. K. *et al.* Gambogic acid, a novel ligand for transferrin receptor, potentiates TNF-induced apoptosis through modulation of the nuclear factor-kappaB signaling pathway. *Blood* **110**, 3517-3525, doi:10.1182/blood-2007-03-079616 (2007).

42 Wang, J. & Pantopoulos, K. Regulation of cellular iron metabolism. *The Biochemical journal* **434**, 365-381, doi:10.1042/BJ20101825 (2011).

43 Moos, T. & Morgan, E. H. The metabolism of neuronal iron and its pathogenic role in neurological disease: review. *Annals of the New York Academy of Sciences* **1012**, 14-26 (2004).

44 Burdo, J. R. & Connor, J. R. Brain iron uptake and homeostatic mechanisms: an overview. *Biometals : an international journal on the role of metal ions in biology, biochemistry, and medicine* **16**, 63-75 (2003).

45 Luck, A. N. & Mason, A. B. Transferrin-mediated cellular iron delivery. *Current topics in membranes* **69**, 3-35, doi:10.1016/B978-0-12-394390-3.00001-X (2012).

46 Aisen, P., Enns, C. & Wessling-Resnick, M. Chemistry and biology of eukaryotic iron metabolism. *The international journal of biochemistry & cell biology* **33**, 940-959 (2001).

47 Loreal, O. *et al.* Iron, hepcidin, and the metal connection. *Frontiers in pharmacology* **5**, 128, doi:10.3389/fphar.2014.00128 (2014).

48 Jing, S. Q. & Trowbridge, I. S. Identification of the intermolecular disulfide bonds of the human transferrin receptor and its lipid-attachment site. *The EMBO journal* **6**, 327-331 (1987).

49 Alvarez, E., Girones, N. & Davis, R. J. Inhibition of the receptor-mediated endocytosis of diferric transferrin is associated with the covalent modification of the transferrin receptor with palmitic acid. *The Journal of biological chemistry* **265**, 16644-16655 (1990).

50 Gkouvatsos, K., Papanikolaou, G. & Pantopoulos, K. Regulation of iron transport and the role of transferrin. *Biochimica et biophysica acta* **1820**, 188-202, doi:10.1016/j.bbagen.2011.10.013 (2012).

51 Zhao, N. & Enns, C. A. Iron transport machinery of human cells: players and their interactions. *Current topics in membranes* **69**, 67-93, doi:10.1016/B978-0-12-394390-3.00003-3 (2012).

52 Richardson, D. R. *et al.* Mitochondrial iron trafficking and the integration of iron metabolism between the mitochondrion and cytosol. *Proceedings of the National Academy of Sciences of the United States of America* **107**, 10775-10782, doi:10.1073/pnas.0912925107 (2010).

53 Chen, H. *et al.* Mitofusins Mfn1 and Mfn2 coordinately regulate mitochondrial fusion and are essential for embryonic development. *The Journal of cell biology* **160**, 189-200, doi:10.1083/jcb.200211046 (2003).

54 Twig, G. *et al.* Tagging and tracking individual networks within a complex mitochondrial web with photoactivatable GFP. *American journal of physiology. Cell physiology* **291**, C176-184, doi:10.1152/ajpcell.00348.2005 (2006).

55 Xu, X. *et al.* Insulin Signaling Regulates Fatty Acid Catabolism at the Level of CoA Activation. *PLoS genetics* **8**, e1002478, doi:10.1371/journal.pgen.1002478
PGENETICS-D-11-01312 [pii] (2012).

56 Pappas, A., Anthonavage, M. & Gordon, J. S. Metabolic fate and selective utilization of major fatty acids in human sebaceous gland. *The Journal of investigative dermatology* **118**, 164-171, doi:10.1046/j.0022-202x.2001.01612.x (2002).

57 Cham, B. E. & Knowles, B. R. A solvent system for delipidation of plasma or serum without protein precipitation. *Journal of lipid research* **17**, 176-181 (1976).

58 Jung, A., Hollmann, M. & Schafer, M. A. The fatty acid elongase NOA is necessary for viability and has a somatic role in Drosophila sperm development. *Journal of cell science* **120**, 2924-2934, doi:10.1242/jcs.006551 (2007).

59 Fernandez-Ayala, D. J. *et al.* Expression of the Ciona intestinalis alternative oxidase (AOX) in Drosophila complements defects in mitochondrial oxidative phosphorylation. *Cell metabolism* **9**, 449-460, doi:10.1016/j.cmet.2009.03.004 (2009).

60 Tiefenbock, S. K., Baltzer, C., Egli, N. A. & Frei, C. The Drosophila PGC-1 homologue Spargel coordinates mitochondrial activity to insulin signalling. *The EMBO journal* **29**, 171-183, doi:10.1038/emboj.2009.330 (2010).

61 Greene, J. C. *et al.* Mitochondrial pathology and apoptotic muscle degeneration in Drosophila parkin mutants. *Proceedings of the National Academy of Sciences of the United States of America* **100**, 4078-4083, doi:10.1073/pnas.0737556100 (2003).

62 Park, J. *et al.* Mitochondrial dysfunction in Drosophila PINK1 mutants is complemented by parkin. *Nature* **441**, 1157-1161, doi:10.1038/nature04788 (2006).

63 Morais, V. A. *et al.* PINK1 loss-of-function mutations affect mitochondrial complex I activity via NdufA10 ubiquinone uncoupling. *Science* **344**, 203-207, doi:10.1126/science.1249161 (2014).

64 Morrison, W. R. & Smith, L. M. Preparation of Fatty Acid Methyl Esters and Dimethylacetals from Lipids with Boron Fluoride--Methanol. *Journal of lipid research* **5**, 600-608 (1964).

65 Jump, D. B. Mammalian fatty acid elongases. *Methods in molecular biology* **579**, 375-389, doi:10.1007/978-1-60761-322-0_19 (2009).

66 Pesta, D. & Gnaiger, E. High-resolution respirometry: OXPHOS protocols for human cells and permeabilized fibers from small biopsies of human muscle. *Methods in molecular biology* **810**, 25-58, doi:10.1007/978-1-61779-382-0_3 (2012).

67 Guitart, T. *et al.* New aminoacyl-tRNA synthetase-like protein in insecta with an essential mitochondrial function. *The Journal of biological chemistry* **285**, 38157-38166, doi:10.1074/jbc.M110.167486 (2010).

68 Bolte, S. & Cordelieres, F. P. A guided tour into subcellular colocalization analysis in light microscopy. *Journal of microscopy* **224**, 213-232, doi:JMI1706 [pii]
10.1111/j.1365-2818.2006.01706.x (2006).

69 Rehman, J. *et al.* Inhibition of mitochondrial fission prevents cell cycle progression in lung cancer. *FASEB journal : official publication of the Federation of American Societies for Experimental Biology* **26**, 2175-2186, doi:10.1096/fj.11-196543 (2012).

70 Wieckowski, M. R., Giorgi, C., Lebiedzinska, M., Duszynski, J. & Pinton, P. Isolation of mitochondria-associated membranes and mitochondria from animal tissues and cells. *Nature protocols* **4**, 1582-1590, doi:10.1038/nprot.2009.151 (2009).

71 Shi, T., Wang, F., Stieren, E. & Tong, Q. SIRT3, a mitochondrial sirtuin deacetylase, regulates mitochondrial function and thermogenesis in brown adipocytes. *The Journal of biological chemistry* **280**, 13560-13567, doi:10.1074/jbc.M414670200 (2005).

72 Park, J. *et al.* Drosophila Porin/VDAC affects mitochondrial morphology. *PloS one* **5**, e13151, doi:10.1371/journal.pone.0013151 (2010).

73 Sheftel, A. D. *et al.* The human mitochondrial ISCA1, ISCA2, and IBA57 proteins are required for [4Fe-4S] protein maturation. *Molecular biology of the cell* **23**, 1157-1166, doi:10.1091/mbc.E11-09-0772 (2012).

74 Morales-Serna, J. A. *et al.* Synthesis of Hyperbranched β-Galceramide-Containing Dendritic Polymers that Bind HIV-1 rgp120. *European Journal*

of Organic Chemistry **2010**, 2657-2660, doi:10.1002/ejoc.201000132 (2010).

75 Hang, H. C. *et al.* Chemical Probes for the Rapid Detection of Fatty-Acylated Proteins in Mammalian Cells. *Journal of the American Chemical Society* **129**, 2744-2745, doi:10.1021/ja0685001 (2007).

76 Lumbroso, A., Abermil, N. & Breit, B. Atom economic macrolactonization and lactonization viaredox-neutral rhodium-catalyzed coupling of terminal alkynes with carboxylic acids. *Chemical Science* **3**, 789-793, doi:10.1039/C2SC00812B (2012).

77 Schagger, H. Tricine-SDS-PAGE. *Nature protocols* **1**, 16-22, doi:10.1038/nprot.2006.4 (2006).

4. Complete, uncropped western blots

Supplementary Figures 12 – 20 follow on the next pages, containing the complete, uncropped western blots presented in this manuscript. In each uncropped figure, the figure panel number of the corresponding cropped figure (either main figure or extended data figure) is indicated.

Supplementary Figure 12

3e

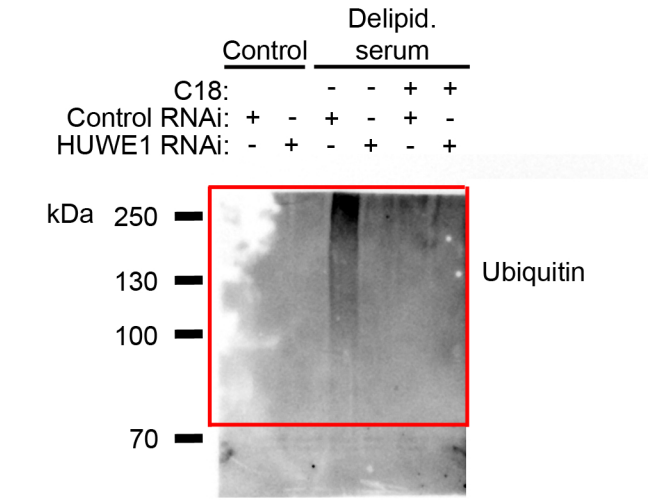

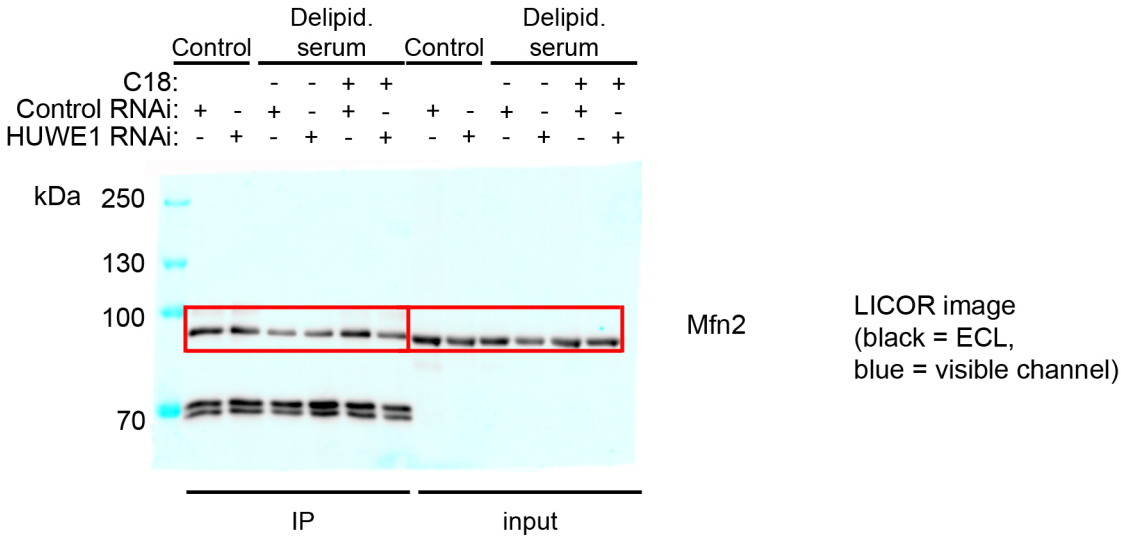

ED1h

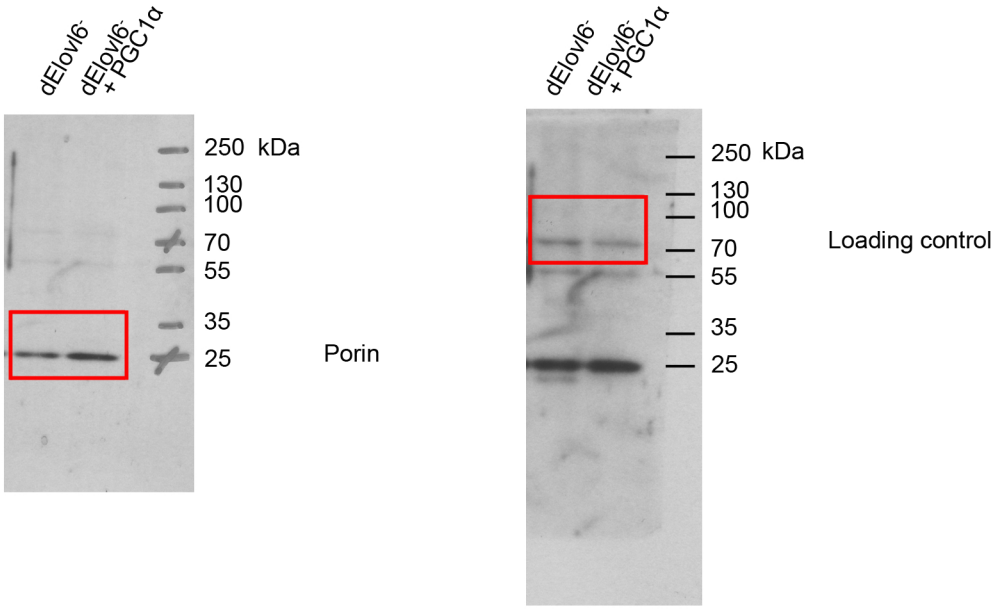

Supplementary Figure 13

ED1j

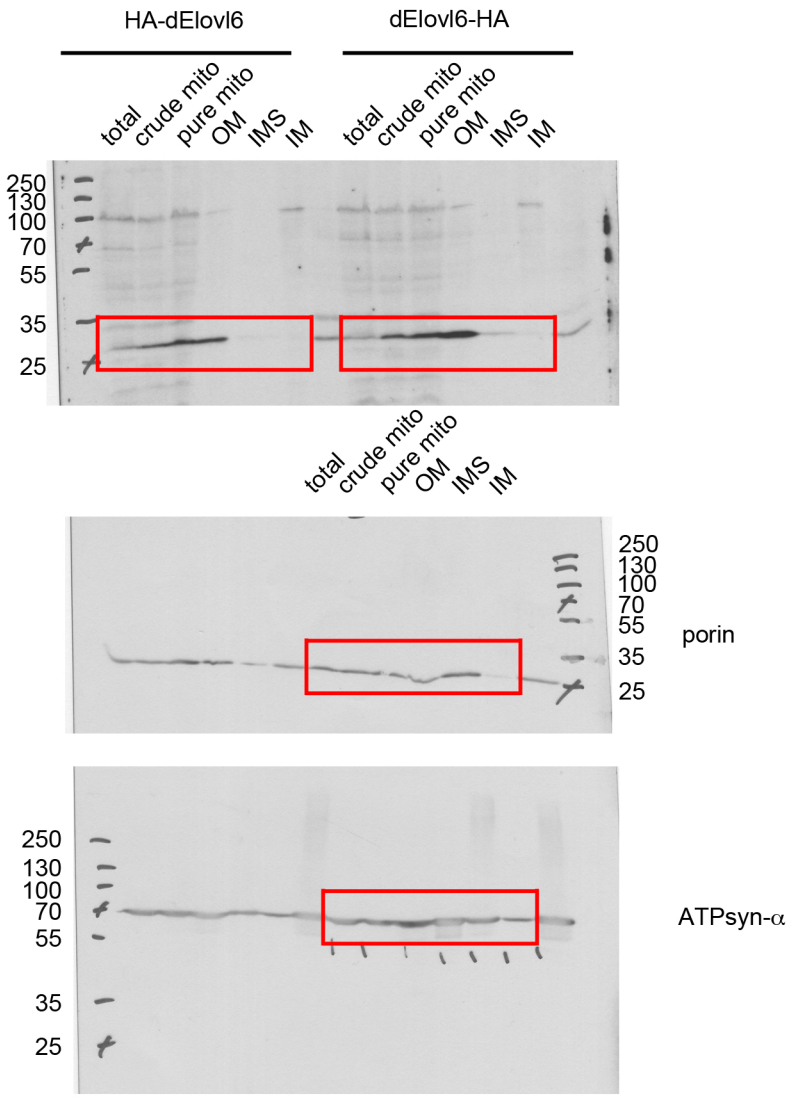

Supplementary Figure 14

ED2b

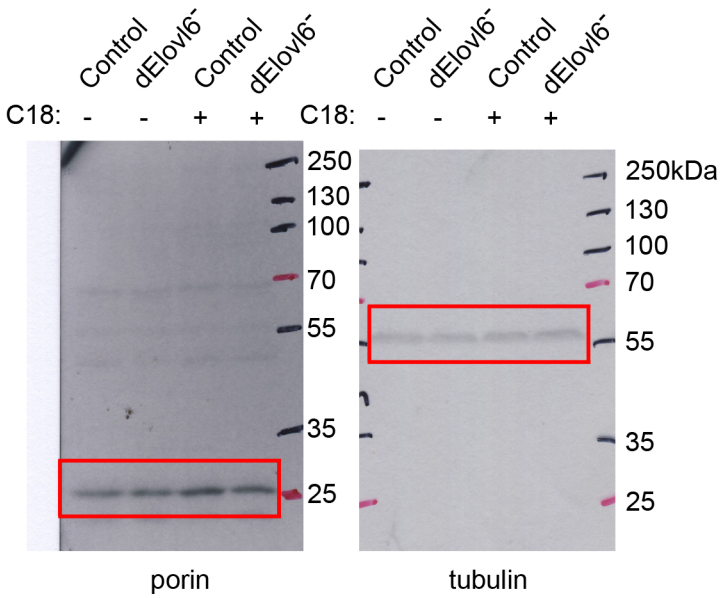

ED2f”

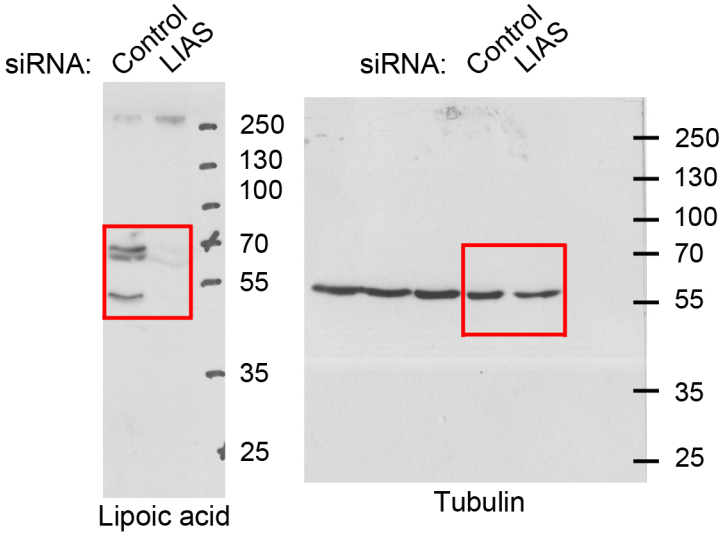

Supplementary Figure 15

ED2g & h(same extracts)

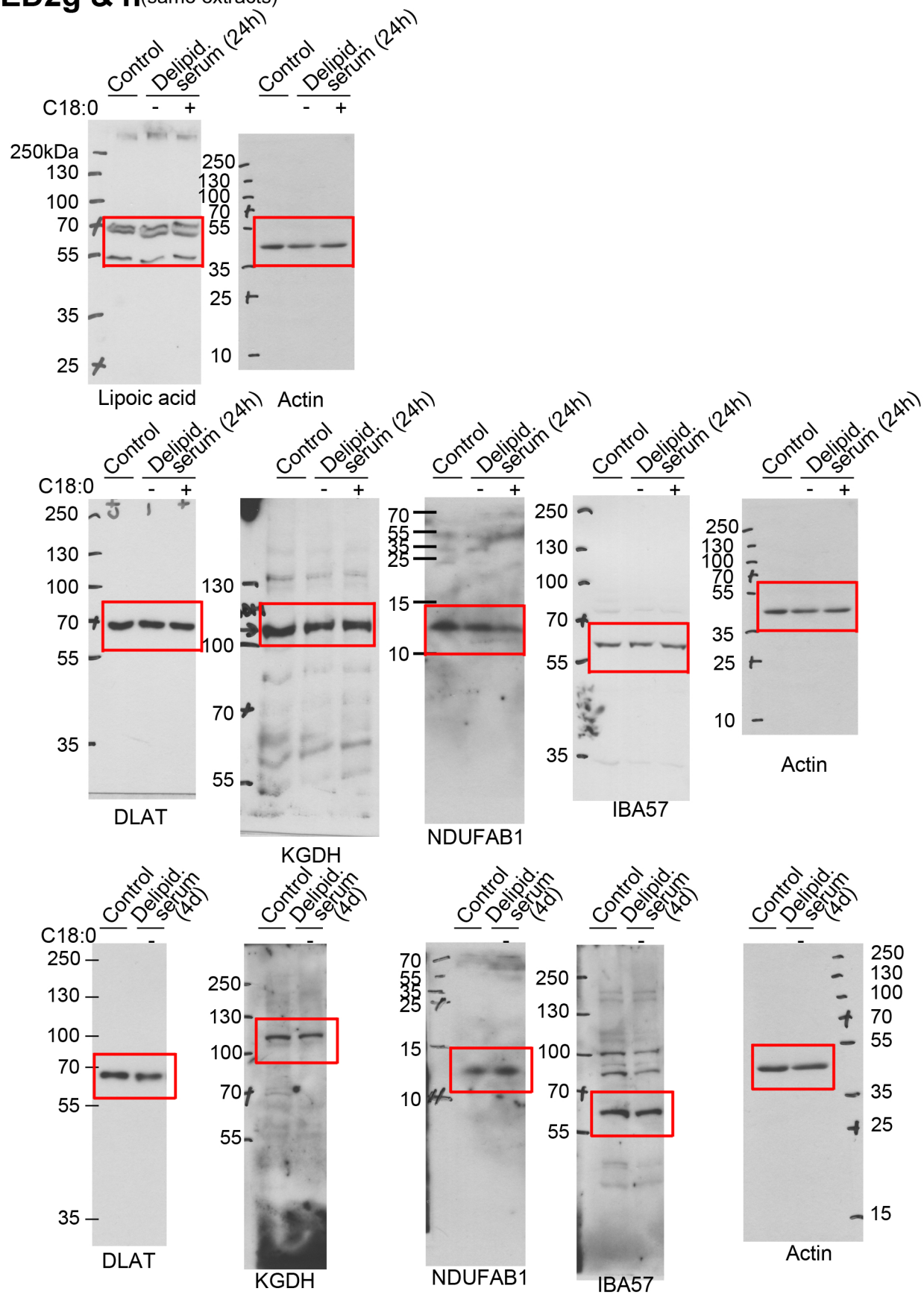

Supplementary Figure 16

ED 3b

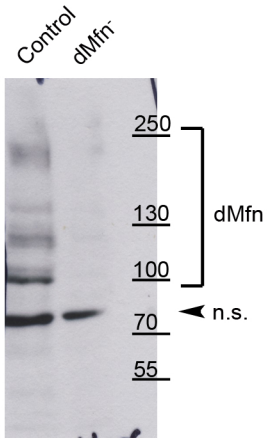

ED 3e

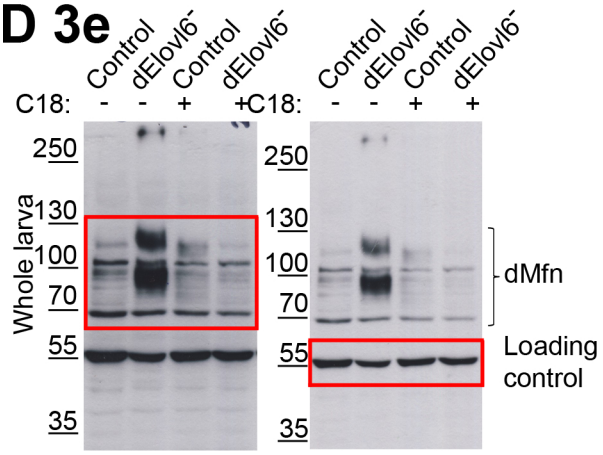

ED 3f

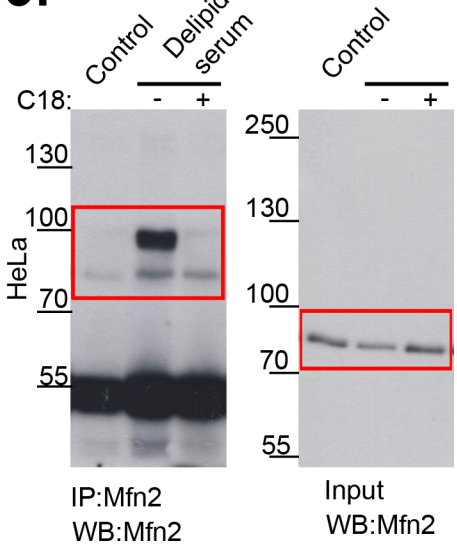

ED 3g

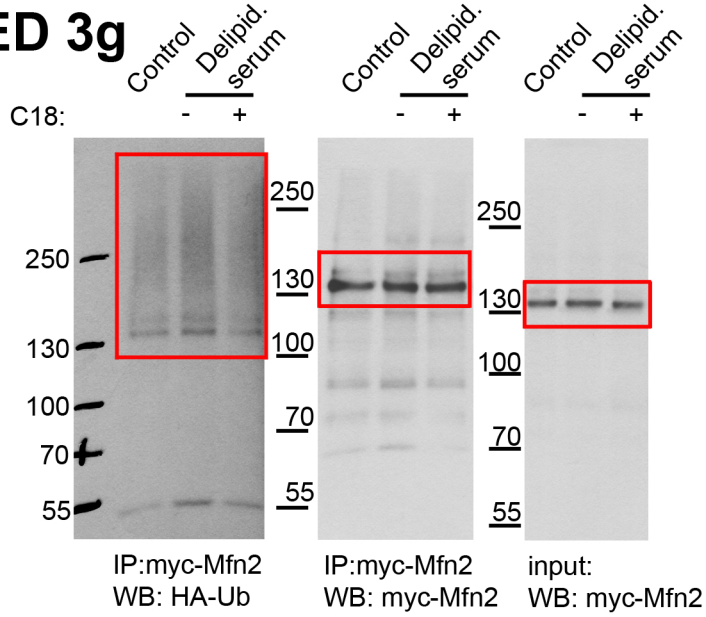

ED 3h

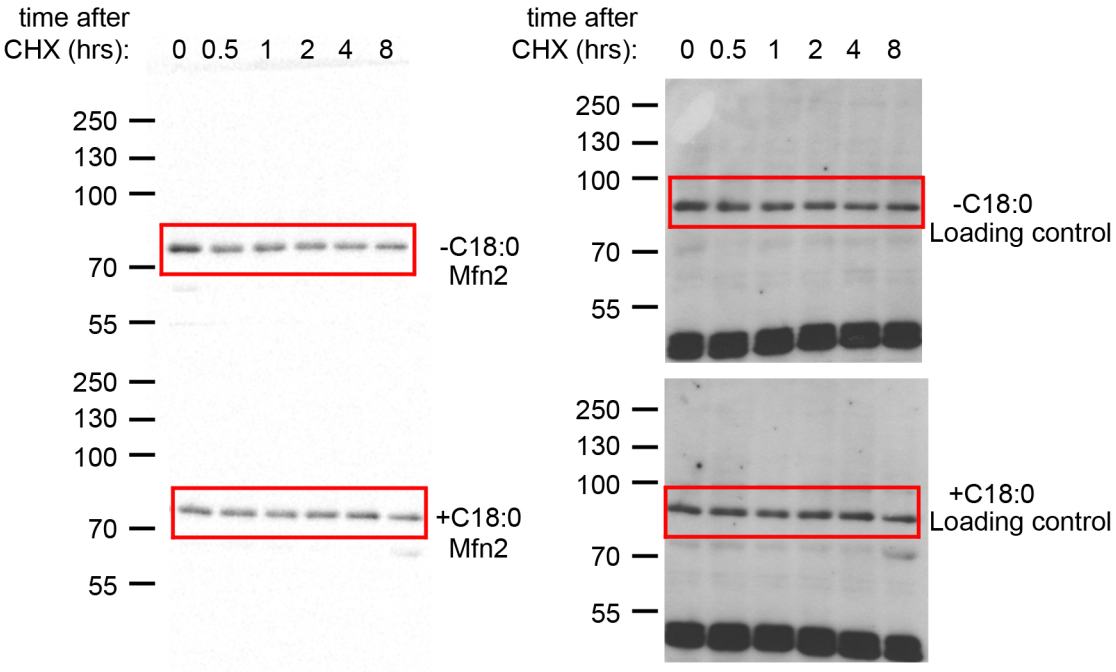

Supplementary Figure 17

ED 5b

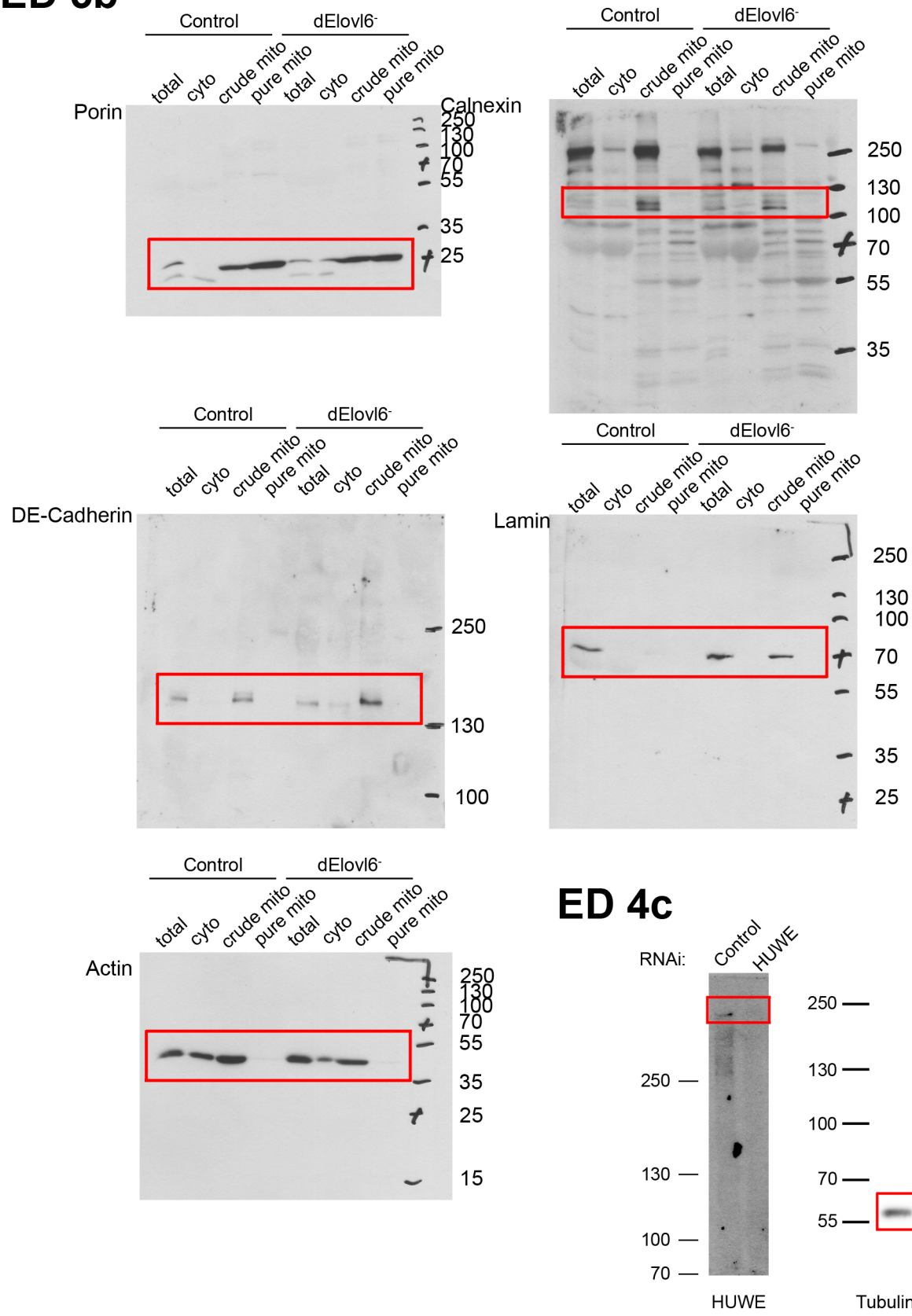

ED 4c

Supplementary Figure 18

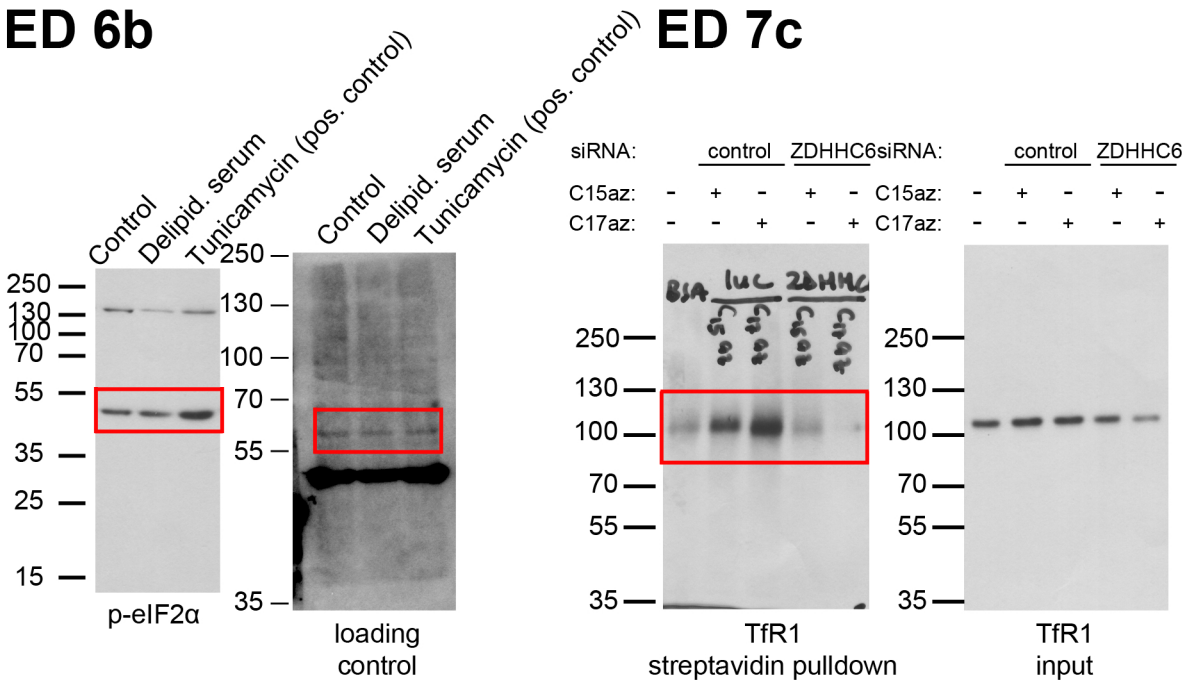

Supplementary Figure 19

ED 8c

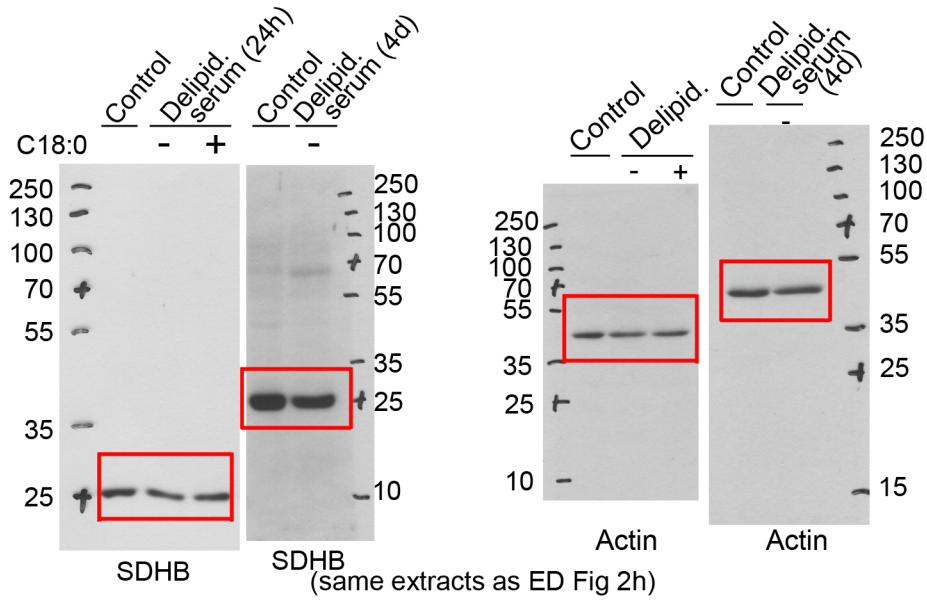

(same extracts as ED Fig 2h)

ED 8h

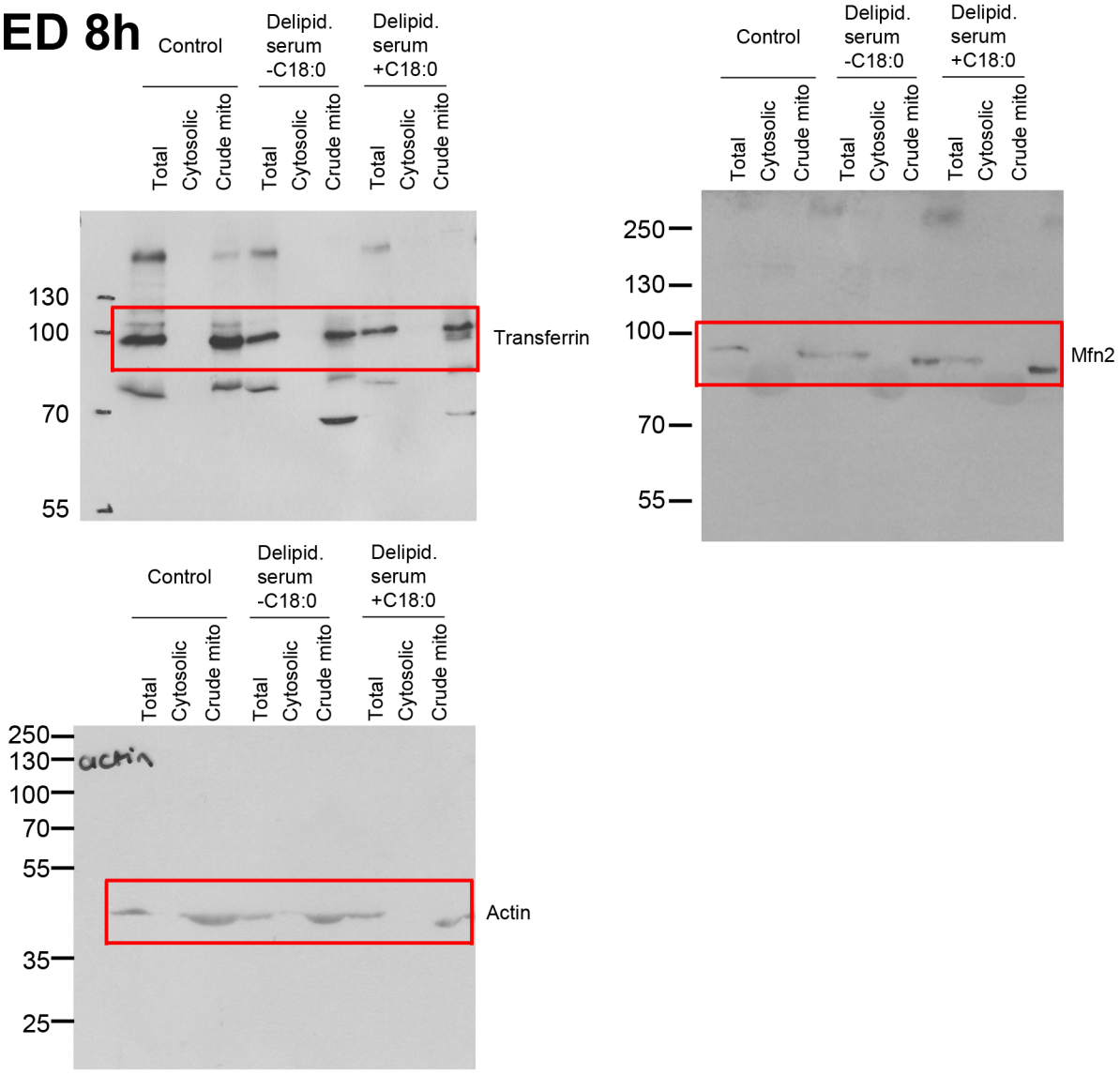

Supplementary Figure 20

ED 9a

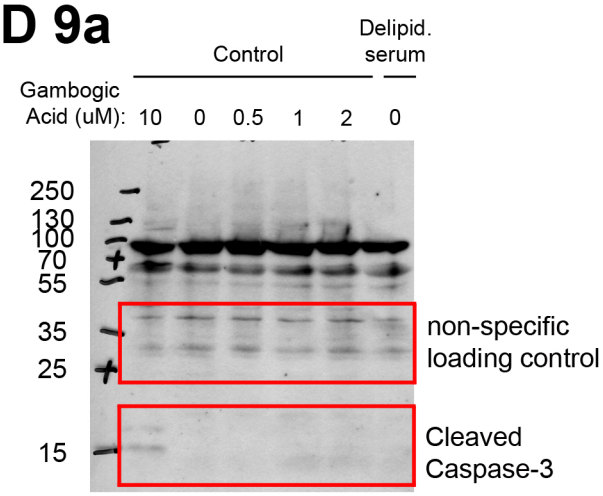

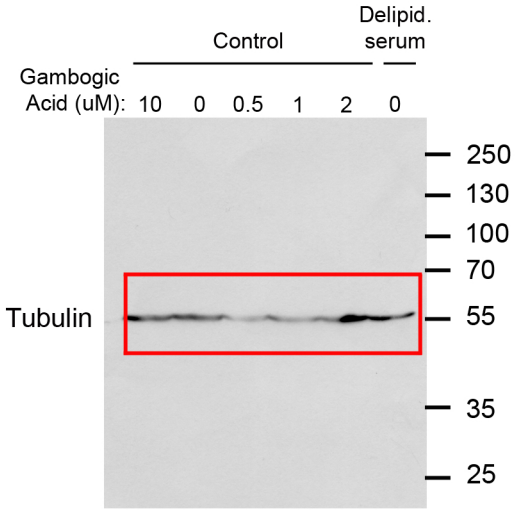

ED 9c

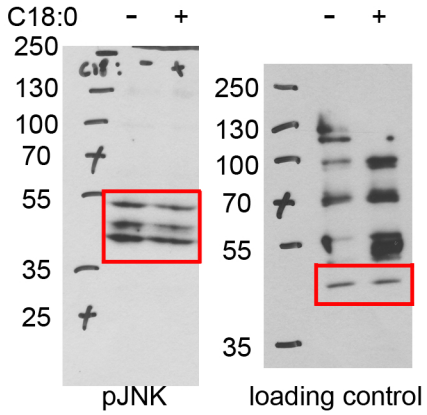

(If anything, the '+' lane has more protein than the '-'. The most conservative band, showing equal amounts, was chosen.)